Analysis of the Detection of Organophosphate Pesticides in Aqueous Solutions Using Polymer-Coated Single IDT Sensors

Michael J. McCarthy
Marquette University

ANALYSIS OF THE DETECTION OF ORGANOPHOSPHATE PESTICIDES IN AQUEOUS SOLUTIONS USING POLYMER-COATED SINGLE IDT SENSORS

By

Michael McCarthy, B.S.

A Thesis submitted to the Faculty of the Graduate School,
Marquette University,
in Partial Fulfillment of the Requirements for
the Degree of Master of Science

Milwaukee, Wisconsin

August 2014

ABSTRACT

ANALYSIS OF THE DETECTION OF ORGANOPHOSPHATE PESTICIDES IN AQUEOUS SOLUTIONS USING POLYMER-COATED SINGLE IDT SENSORS

Michael McCarthy, B.S.

Marquette University, 2013

The single interdigital transducer (IDT) device was investigated as a micro-chemical sensor for the detection of organophosphates compounds in aqueous solutions. The compounds of interest are: parathion, parathion-methyl, and paraoxon. The polymers used as a partially-selective coating for the direct detection of these compounds are 2,2'-diallylbisphenol A- 1,1,3,3,5,5-hexamethyltrisiloxane (BPA-HMTS) and polyepichlorohydrin (PECH). BPA-HMTS is synthesized here at Marquette University.

The measurement of interest for the single IDT is the change radiation resistance. The radiation resistance represents the energy stored in the propagating acoustic wave. As analyte absorbs into the polymer coating, changes in the film's properties will undergo resulting in a change in the radiation resistance i.e the acoustic wave properties. The film's properties changing include: added mass, viscoelastic properties, thickness, and dielectric properties. These properties will contribute to an overall change in the radiation resistance. A linear change in the radiation resistance is expected to occur for increasing concentrations of an organophosphate.

The experimental results indicate that BPA-HMTS shows greater sensitivity towards the organophosphates than PECH. Both polymers showed greatest to lowest sensitivity to parathion, parathion-methyl, and paraoxon respectively. Thicker films tested for both polymers, 0.75μm thick, show a higher response due to a more pronounced effect of mass loading than the thinner films tested, 0.50μm. The response times for BPA-HMTS were much faster than for PECH. Both films showed fastest to slowest response time to paraoxon, parathion-methyl, and parathion respectively.

The sensor is tested for reproducibility for the polymer BP-HMTS. A sensor array consisting of separately tested devices from this work as well as work done by a previous student is utilized to increase the selectivity of the three organophosphates. Radial plots are performed for each organophosphate and concentration using the change in radiation resistance, response time, and frequency shift for both BPA-HMTS and PECH at 0.50μm as input parameters. These plots yield unique recognition patterns for each organophosphate that can be used to distinguish one from another.

ACKNOWLEDGEMENTS

Michael McCarthy, B.S.

I would like to thank my mother for supporting me throughout my entire academic career. Without your encouragement and help, I could not have made it this far.

I would also like to thank Dr. Fabien Josse for the time and support he has invested in me to move forward and complete my Master's thesis. I would also like to thank Dr. Florian Bender for his help in the lab and for feedback on my thesis. Also, I want to thank Dr. Chung-Hoon Lee for his advice and insight at the seminar meetings. And finally I want to thank my colleagues Tian Newman, Robert Lenisa, and Jude Coompson for their help and feedback.

TABLE OF CONTENTS

1. INTRODUCTION

1.1 Background

The term organophosphates (OPs) in health and agriculture refers to a group of organic compounds which contain phosphorus. Some of these organic compounds are used as pesticides or fertilizers. Organophosphate pesticides act irreversibly on the acetylcholinesterase enzyme which is essential to nerve function in insects, humans, and other animals [1]. OPs are chemical compounds that are produced by reacting alcohols and phosphoric acid and are considered toxic to humans even at very low levels of exposure [2].

Organophosphates were a popular choice for insecticides because they degrade very rapidly upon exposure to sunlight, air, and soil; however, small amounts can still be detected in food and drinking water. Their ability to degrade made them an attractive choice over organochloride pesticides, formerly used [2]. Though they degrade more rapidly they are much more toxic. Their toxicity to humans was exploited for the development of chemical warfare agents in World War II [3].

Even at relatively low levels, organophosphates can be hazardous to human health. They are a common cause of poisoning worldwide [2]. Organophosphorous pesticides can be absorbed by ingestion, inhalation, and dermal absorption [4]. The most common ways people are exposed to these pesticides is by eating them on foods or drinking them from contaminated water sources.

Pesticide contamination of groundwater is a subject of national importance because ground water is used as drinking water by about 50 percent of the population [5]. This is especially a concern for those that live in rural areas where pesticides are more often used. Pesticides can reach water sources below ground from applications on crop fields, spills, or improper disposal. Though many dangerous pesticides are banned by the Environmental Protection Agency (EPA), trace pesticides can show up in ground water decades after they were originally used [5]. This requires the need to currently monitor OPs in ground water so that preventative actions can be taken.

Traditional methods for the detection of OPs require samples to be taken to a laboratory for analysis [6]. These methods are costly and time consuming. Because OPs degrade very rapidly, sometimes vital information is lost when samples are being transported [2]. Therefore, there is the need for a portable, cheap, and reusable sensor capable of making on-site, real-time measurements of the detection and classification of OPs.

1.2 Overview of Chemical Sensors

A sensor is a transducer that measures a physical or chemical quantity and converts it into a signal that can be processed, usually an electrical signal [7]. A sensor responds to an input by generating a related electrical signal. By considering the nature of the input, sensors can be classified as either physical or chemical. The measurand of a physical sensor is a physical quantity such as mass, velocity, or temperature.

A chemical sensor is a device which converts chemical information into an electrical signal. The chemical information can range from the concentration of a

specific sample to total composition analysis [7]. The chemical information extracted may originate from a chemical reaction or from a physical property of the system. In addition to the sensor itself, the sensor system may include other devices that perform functions such as sampling, monitoring, data acquisition, and signal processing [8].

Chemical sensors are comprised of two functioning units, the receptor and transducer. The receptor will take the chemical information and transform it into an energy form that can be measured by the transducer. The transducer will transform the energy carrying the chemical information into a useful analytical signal. The receptor shows selectivity but the transducer does not. The receptor on a chemical sensor can be based on various principles: physical, chemical, or biochemical. Examples of physical processes are based on measuring the change in absorbance, refractive index, temperature, or mass. Chemical processes involve a reaction with the analyte of choice which gives rise to a useful signal. Biochemical processes as well can be the source of an analytical signal; an example is the immunosensor [9].

Chemical sensors can further be classified by certain criterion. Sensors can be considered as modulating (active) or self-generating (passive). Active sensors require an auxiliary power source whereas passive sensors do not [10].

Important parameters to consider when designing a chemical sensor include sensitivity, selectivity, and reproducibility. Quantitatively, sensitivity is the slope of the calibration curve along the measurement range. For a sensor in which output y is related to the input x by the equation $y = f(x)$, the sensitivity $S(x_a)$ at point x_a is given by [10]

$$S(x_a) = \left.\frac{dy}{dx}\right|_{x=x_a}$$

Qualitatively, sensitivity describes the change in the output per unit change in the parameter being measured. Selectivity describes the degree to which the sensor can distinguish target species from non-target species. Reproducibility is the closeness of agreement between successive results obtained with the same method under the same conditions during a long-term set of measurements [10].

There are various sensor technologies that can be used to implement chemical sensors. They are classified according to the operating principle of their transducer. Examples are optical, electrochemical, magnetic, chemiresistive, acoustic wave, and many more [7]. The surface acoustic wave sensor will be the sensor of interest for this work and will be discussed in more detail. Acoustic wave devices offer many advantages over other sensor technologies and have found a use for chemical sensing.

1.3 Acoustic Wave Devices

The phenomenon of surface acoustic wave (SAW) propagation was first discovered by Lord Rayleigh in 1885 [11]. Termed “Rayleigh Waves” but better known as SAW, are acoustic waves that travel along the surface of solids. A SAW has both a longitudinal and vertical shear component such that the particles are moving both parallel and perpendicular to the direction of wave propagation in an elliptical fashion. The penetration depth is about one wavelength for SAWs [12].

The application of SAW devices in electronics did not occur until the 60’s when they were first used as electronic filters and for analog signal-processing applications [11]. From there they found wide application in other fields such as communications, automotive, commercial applications, and more recently chemical sensing. The

interaction between the SAW and an outside media strongly affects the properties of the wave which has been exploited for sensing [11]. The first acoustic wave sensor was the Quartz Crystal Microbalance (QCM) which was originally designed to measure film thickness in IC fabrication by measuring the added mass [13]. It was later discovered that SAW devices could be used as chemical sensors by utilizing a chemically-selective film coating [14].

Virtually all SAW sensors use the principle of the piezoelectric effect. The piezoelectric effect is the generation of a mechanical stress by an applied electric field [15]. If the electric field is periodic, the same applies to the mechanical stress, resulting in the generation of an acoustic wave. Likewise, the piezoelectric effect can work inversely to convert a mechanical wave back into an electric field. The piezoelectric effect will occur only on a piezoelectric material. The QCM was designed using a piezoelectric substrate "sandwiched" between two electrodes. When the two electrodes are fed an AC signal, a standing bulk acoustic wave (BAW) is generated between the two crystal surfaces. This allows the device to sense changes at the surface, such as mass loading [12].

Acoustic waves are differentiated by their velocity and mode of propagation. The three different modes of particle displacement are longitudinal, shear-horizontal, and shear-vertical [12]. Furthermore, there are surface acoustic waves (SAW) and bulk acoustic waves (BAW). Longitudinal waves have particle displacement parallel to the direction of the wave, shear-vertical waves have particle displacement normal to the surface and the direction of wave propagation, and shear-horizontal waves have particle displacement parallel to the surface but perpendicular to the direction of the wave. An

acoustic wave can be one or a combination of the three. The SAW is a combination of a longitudinal and shear-vertical wave. Which acoustic mode can propagate on a particular substrate depends on the piezoelectric material and the angle at which the crystal is cut. An acoustic wave that travels through the substrate and is not confined to the surface is called bulk acoustic waves (BAW) [10]. The QCM is an example of a BAW device.

An acoustic wave device cannot have a shear-vertical component for sensing in liquid. The wave energy would dissipate into the liquid medium causing excessive attenuation and loss, making it unsuitable for sensing. For this reason, only longitudinal and shear-horizontal modes can be used for liquid sensing [12].

The development of acoustic wave sensors was improved upon the invention of the interdigital transducer (IDT) [12]. The interdigital transducer brought a more efficient method of converting electrical energy into acoustic energy [15]. Devices fabricated using an interdigital transducer are: the surface-acoustic wave (SAW) device, the flexural-plate wave (FPW) device, shear-horizontal surface acoustic wave (SH-SAW) device, and shear-horizontal acoustic plate mode (SH-APM) device. A brief review of the interdigital transducer will be discussed in the next section.

1.4 The Interdigital Transducer

A major factor in the emergence of SAW devices was the invention of the interdigital transducer (IDT). The IDT allows for efficient transduction of electrical energy to acoustic energy. This transducer formed the basis for a variety of SAW devices such as delay lines, filters, and sensors [15].

The interdigital transducer consists of a series of interleaved electrode fingers made from a metal film deposited on a piezoelectric substrate. An applied voltage will cause, through the piezoelectric effect, a strain pattern. If the frequency is such that the wavelength of the surface wave is equal to the periodicity of the transducer, there is strong coupling [16]. The stress pattern excited by the transducer corresponds to the sum of the stress of the two oppositely traveling waves, resulting in a standing-wave stress pattern [15]. The theory and transduction mechanism behind the interdigital transducer is reviewed and presented in more detail in Chapter 2.

Surface acoustic wave sensors utilizing a delay line have two IDTs, one on each end. The input IDT will convert an electrical signal into an acoustic wave launched in the direction towards the output IDT. The output IDT will then convert the acoustic wave back into an electrical signal for analysis. The changes in the properties of the wave resulting from perturbations along the delay line would be measured and used as a sensing mechanism [17]. The interdigital transducer by itself can be exploited for sensing, too; this approach will be used in this work. Various properties of the transducer can be perturbed to make a suitable sensor in liquid. These properties include the radiation resistance, capacitance, and frequency shift and will be discussed in more detail in Chapter 2. Using a single IDT for chemical sensor will reduce the overall size of the sensor device as well as offer different unique properties to be monitored for sensing.

1.5 Problem Statement and Objective of Research

Presently, there are no systems on the market to directly detect organophosphates in-situ. Current alternatives are to take test samples from a source and transport them to a

laboratory for testing and analysis [6]. These methods are both cumbersome and time-consuming. In addition, transportation of test samples can cause vital information to be lost during the process. Therefore, a sensor capable of making real-time measurements on site is desired [2].

The goal of this thesis is to investigate and design micro-chemical sensors for the detection of OPs in aqueous environments. The sensor platform that will be used in this work will be a single interdigital transducer on a piezoelectric substrate supporting a shear-horizontal surface acoustic wave. The sensor will utilize a partially selective polymer coating on top of the transducer to allow for perturbation of the electrical and mechanical properties at the surface for the detection of key pesticides. This work will investigate two different selective polymers: polyepichlorohydrin (PECH) and 2,2'-diallylbisphenol A – 1,1,3,3,5,5-hexamethyltrisiloxane (BPA-HMTS). Both films will be tested in terms of their sensitivity, response time, and reusability for the pesticides of interest: parathion, parathion-methyl, and paraoxon [18].

For a large number of chemical sensing applications, a single sensor is not sufficient to adequately characterize the environment. Rather, a sensor array is needed. This can be complemented by using steady-state and response time information to increase the selectivity of the sensor system. It would be beneficial to have one device that contains multiple coated transducers to sense the three pesticides. To design such an array, one needs to identify optimal thicknesses of the selected film for each of the three pesticides. This work will be presenting results and data collected from experiments on organophosphate detection with the two selected polymer films. This research can then be used for the design and fabrication of an effective sensor array.

1.6 Thesis Organization

This thesis consists of five chapters. Chapter 1 is a brief introduction to the pesticide problem, chemical sensors and their classifications, the interdigital transducer, and the goal of this research. In Chapter 2, the theory of the interdigital transducer will be reviewed and discussed in greater detail. An explanation of the sensing mechanism behind the IDT as well as an equivalent circuit model to represent the IDT will be discussed. Chapter 3 will contain a description of the three pesticides and two polymer films used in this work and descriptions of the experimental set-ups, procedures, and instruments. Chapter 4 will focus on the results and analysis. Data collected for the sensor array will be presented and discussed. Sensitivities for the measurements will be determined. The two polymer films will also be compared in terms of their sensitivity to the three organophosphate pesticides. Chapter 5 will consist of a summary, conclusion, and possible future work on this subject.

2. MODELING OF THE IDT AS A LIQUID-PHASE SENSOR ELEMENT

2.1 Introduction to the IDT

As mentioned in Chapter 1, the advancement in acoustic wave devices was due to the invention of the IDT. The IDT allows for efficient conversion of electrical energy to acoustic energy and vice versa. In this chapter the IDT will be examined more closely. First, the geometry and principle of operation will be discussed. Then, a review of a mathematical model will be presented to represent the IDT as a simple equivalent circuit. This model will simplify the complexity of the IDT problem. The dielectric film loaded case will then be investigated since this work involves using a selective film for sensing. Finally, the case in which the properties of the dielectric film change will be discussed as it relates to chemical sensing.

2.2 IDT Geometry

The interdigital transducer consists of a series of interleaved electrode fingers made from a thin metal film deposited on a piezoelectric substrate [15]. Fig. 2.1 shows a representation of the IDT. The transducer is considered to have N finger pairs, with period length λ. The width of each electrode is represented as a and the gap width between the IDT fingers is b. The period length is $\lambda = 2a + 2b$. The aperture, W, is the width at which the electrode fingers overlap. The thickness of the electrodes is considered to be negligibly small [16].

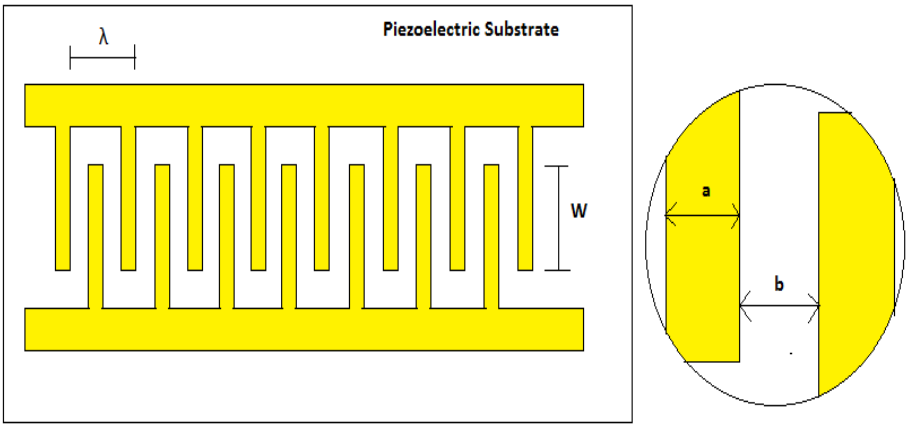

Figure 2.1: Schematic of IDT

In the case of a uniform IDT, the width of the electrodes is equal to the width of the electrode gaps. This doesn't have to be the case when designing an IDT. The relationship between the electrode width and the electrode gap width is given by the metallization ratio, α. The metallization ratio varies from 0 to 1 and is 0.5 for the uniform IDT case. The expression for is given by $\alpha=a/(a+b)$.

2.3 Principle of operation: the piezoelectric effect

The substrate for the IDT must be piezoelectric in order to generate a SAW. The piezoelectric effect is the generation of a mechanical stress from an electric field and vice versa. When an AC signal is applied to the transducer, a time-varying electric field is produced that penetrates into the piezoelectric substrate. This electric field is converted into a mechanical stress which results in effective generation of an acoustic wave if the frequency matches the periodicity of the transducer [19]. An important parameter

regarding piezoelectric materials is the piezoelectric coupling coefficient, k^2. This parameter is a measure of the efficiency at which the electric fields are converted into mechanical fields [21] [22]. Figure 2.2 shows a representation of what the electric fields look like and the resultant SAW.

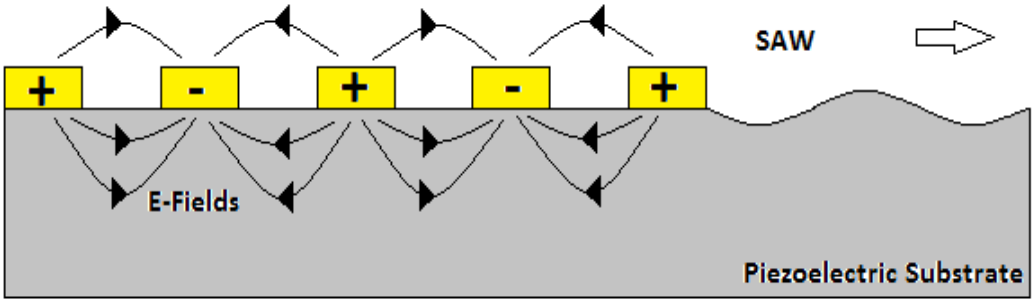

Figure 2.2: Cross-Sectional view of IDT

It is assumed that the electric fields obey the electrostatic approximation from Maxwell's equations and are represented by,

$$D_i = \varepsilon_{ij} E_j \quad i,j = 1,2,3 \qquad (2.1)$$

$$D_{m,m} = 0 \quad m = 1,2,3 \qquad (2.2)$$

where

E_j = the electric field intensity in the X_j direction,

ε_{ij} = the dielectric constant tensor at constant strain

D_m = the electric displacement in the X_m direction.

The repeated indices and comma in the subscripts indicate summation and differentiation with respect to the spatial coordinates respectively.

It is also assumed that the stress and strain are related by [23],

$$T_{ij} = c_{ijkl}S_{kl} \quad i,j,k,l = 1,2,3 \qquad (2.3)$$

$$\rho\ddot{u}_{\iota} = T_{ij,j} \quad i,j = 1,2,3 \qquad (2.4)$$

where

T_{ij} = the acoustic stress tensor

c_{ijkl} = the elasticity matrix at constant electric field

S_{kl} = the strain tensor

ρ = the density of the substrate material

u_i = the acoustic displacement in the X_i direction.

The dots denote differentiation with respect to time.

For piezoelectric materials, the mechanical and electrical properties become coupled. The separate relations of the mechanical and electrical behavior become coupled as,

$$T_{ij} = c_{ijkl}S_{kl} - d_{kij}E_k \qquad (2.5)$$

$$D_i = \varepsilon_{ij}E_j + d_{ijk}S_{jk} \qquad (2.6)$$

The coupling between the two properties is related by the piezoelectric coefficient, d_{kij}. The piezoelectric coefficient is a measure of the strain development from an applied electric field [22]. Combining the definition of strain, the equation of motion, and Maxwell's equations, the Christoffel's wave equations (Eq. 2.7, 2.8) can be obtained to give the appropriate system of coupled wave equations for the electric potential and elastic displacement [24].

$$\rho\ddot{u}_{\iota} = c_{ijkl}u_{k,il} + e_{kij}\phi_{,ik} \qquad (2.7)$$

$$e_{ikl}u_{k,il} - \varepsilon_{ik}\phi_{,ik} = 0 \qquad (2.8)$$

The Christoffel wave equations are sufficient to describe wave propagation in a piezoelectric substrate for the purpose of this thesis. In principle one could solve the boundary conditions to the problem at hand and solve for the coefficients but this is not necessary for this work [22]. Instead, a simplified model will be used to represent the IDT by making use of an equivalent circuit.

2.4 Equivalent Circuit Model of IDT: A Review

Because of the nature and complexity of the IDT, an accurate theory can be very complicated and difficult. Smith et al proposed a theory which considers the transducer as an array of sources, each source being analogous to a piezoelectric plate transducer for launching bulk waves [25]. The significant properties of the transducer can be obtained by breaking the transducer up as an array of individual sources cascaded [25]. One model that fits this theory and will be used in this work is the cross-field model. The cross-field model assumes that the acoustic sources do not interact and has shown good agreement with experimental data [15].

2.4.1 Parallel and Series IDT Representations

The circuit model proposed by Smith et al can be either a parallel or series circuit [25]. The parallel circuit model is known as the cross-field model as represented in Fig 2.3 and the series circuit is known as the in-line model as represented in Fig 2.4. The choice between the two is made by examining the coupled energy stored from the electrical and acoustic fields in the piezoelectric substrate [25].

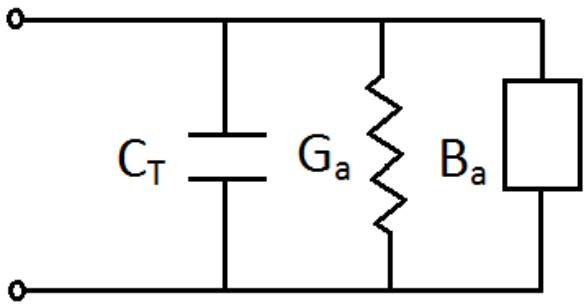

Figure 2.3: Parallel circuit representation of IDT

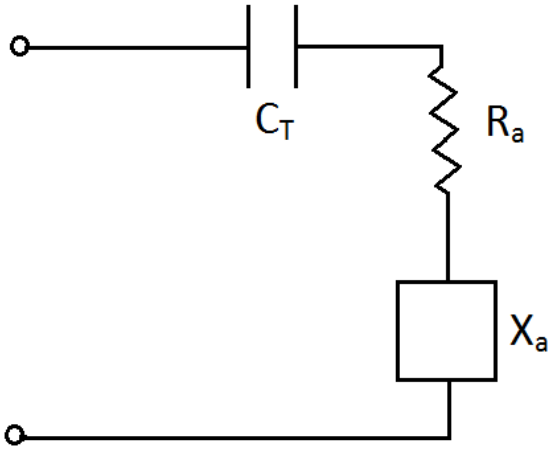

Figure 2.4: Series circuit representation of IDT

The admittance of the transducer for the cross-field model is given by

$$Y_t = G_a(f) + j\left(\omega C_T + B_a(f)\right) \qquad (2.9)$$

where $G_a(f)$ is the radiation conductance, $B_a(f)$ is the radiation susceptance, and C_T is the electrostatic capacitance between the finger pairs. The impedance of the transducer from the in-line model is given by

$$Z_t = R_a(f) + j\left(-\frac{1}{\omega C_T} + X_a(f)\right) \qquad (2.10)$$

where $R_a(f)$ is the radiation resistance and $X_a(f)$ is the radiation reactance.

The choice between the two models depends on the stored coupled energy from the electric and acoustic fields. The electric field approximation for the two models are shown in Fig. 2.5(a) and Fig. 2.5(b). In actuality, the electric field patterns are a combination of the two as shown in Fig. 2.5(c). The distinction between the two is made by examining the parallel and perpendicular components of the electric field pattern. In the cross-field model, the perpendicular component of the electrical field heavily outweighs the parallel component and vice versa for the in-field model. The coupled energy can be numerically described by the equation [25]

$$W_m = \frac{1}{4}\int_V (\boldsymbol{T}^*\!: \boldsymbol{d} \cdot \boldsymbol{E}_\perp + \boldsymbol{E}_\parallel{}^* \cdot \boldsymbol{d}\!: \boldsymbol{T}) d\boldsymbol{V} = W_\perp + W_\parallel \quad (2.11)$$

where $\boldsymbol{d}$ is the piezoelectric stress constant and $\boldsymbol{T}$ is the elastic constant. The mutual stored energy, W_m, can be written as the sum, $W_m = W_\perp + W_\parallel$, where $W_\perp$ and $W_\parallel$ are the energy components related to $E_\perp$ and $E_\parallel$, respectively. The ratio of the energy stored from the perpendicular and parallel components of the electric field distribution are evaluated as $r = \frac{W_\perp}{W_\parallel}$. For $r > 1$, the cross-field model is used and for $r < 1$ the in-line model is used. It has been shown that materials with high piezoelectric coupling are better represented by the cross-field model [25]. Example piezoelectric substrates are $LiTaO_3$ and $LiNbO_3$. Weaker piezoelectric substrates like quartz are more accurately represented using the in-line model. In this work, the piezoelectric substrate of choice is $LiTaO_3$ and so the cross-field model will be closely examined.

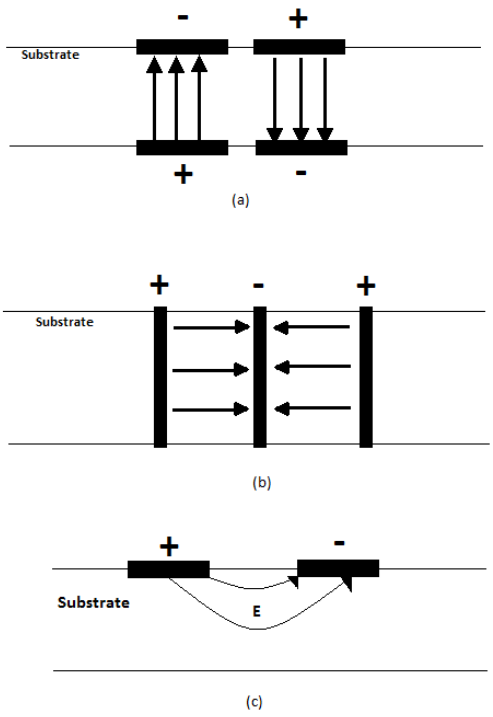

Figure 2.5: Side view of IDT showing field patterns for (a) cross-field model, (b) in-line model, and (c) actual device

2.4.2 Radiation Conductance

In this work, the cross-field model in Fig. 2.3 will be used to represent the IDT as an equivalent circuit. The radiation conductance describes the efficiency of the transducer in generating an acoustic wave from an electrical source. The radiation conductance is proportional to the amount of acoustic power generated from an applied voltage, V_{in}, which is given by the expression [29]

$$G_a = \frac{2P_B}{V_{in}^2} \qquad (2.12)$$

where P_B is the power associated with the excited wave. The power associated with the excited wave is further related by the electromechanical coupling coefficient, k^2. The

electromechanical coupling describes the conversion of electrical energy to mechanical energy for a given substrate.

$$k^2 = \frac{mechanical\ energy\ stored}{electrical\ energy\ applied} \qquad (2.13)$$

For frequencies near the resonant frequency, the radiation conductance and the susceptance are approximately given, respectively, by [15]

$$G_a(\omega) \cong \hat{G}_a \left(\frac{sinx}{x}\right)^2 \qquad (2.14)$$

and the susceptance is

$$B_a(\omega) \cong \hat{G}_a \left(\frac{sin2x-2x}{2x^2}\right) \qquad (2.15)$$

where

$$x = \frac{N\pi(\omega-\omega_o)}{\omega_o} \qquad (2.16)$$

$$\hat{G}_a = \frac{4}{\pi} k^2 \omega_o C_s N^2 \qquad (2.17)$$

where

$\hat{G}_a$ = the radiation conductance at the resonant frequency

k^2 = the electromechanical coupling coefficient

C_s = the electrostatic capacitance associated with a single pair of electrodes

N = the number of finger pairs

Fig. 2.6 shows graphically typical radiation conductance and susceptance curves. The acoustic wave generated can be viewed as the sum of stress contributions from each finger pair [12]. At the resonant frequency, the radiation conductance is maximum because all of the stress contributions are in phase with each other [12]. The susceptance is a measure of how much stress is out of phase with the motion of the wave resulting in a decrease in the overall radiation resistance. As the frequency deviates from the resonant

frequency, the magnitude of the susceptance begins to increase resulting in a decrease in radiation conductance [25].

Graphically, one can solve for the electrostatic capacitance by analyzing the susceptance at the center frequency. At the center frequency, $B_a = 0$, and the value of the nonzero reactance should be equal to $\omega_o C_T$ which is the susceptance from the electrostatic capacitance of the transducer. A more in depth derivation for C_T will be presented in the next section.

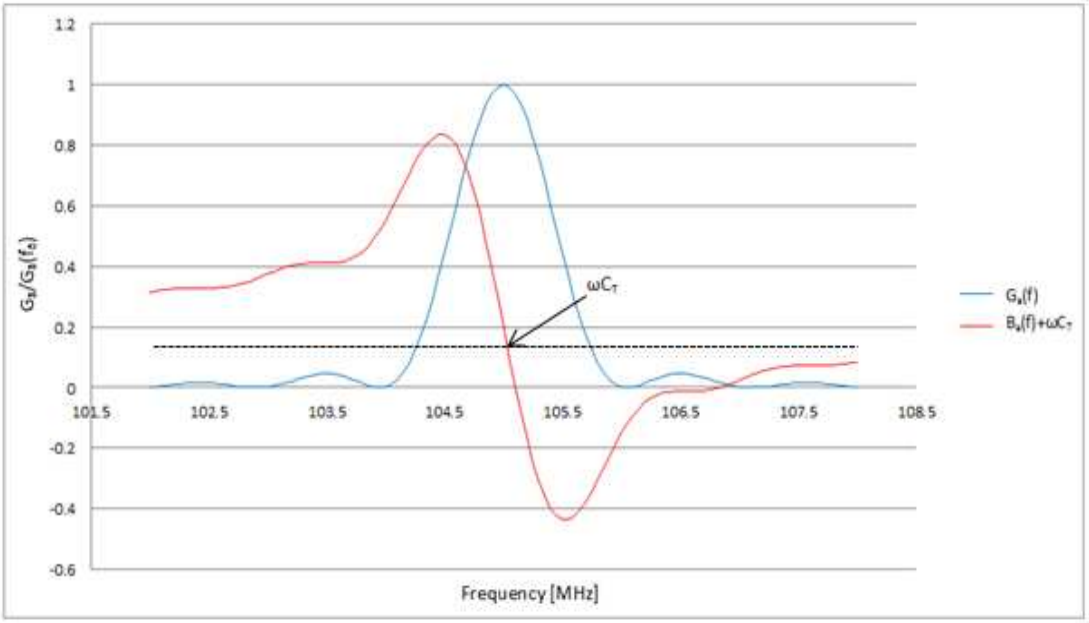

Figure 2.6: Theoretical curves for the radiation conductance and susceptance for example IDT (f=105 MHz)

2.4.3 Electrostatic Capacitance

Calculation of the electrostatic capacitance can be achieved by considering the contributions from the surface charges on the top, bottom, and side surfaces of each IDT

finger. Simplification for deriving the electrostatic capacitance can be done by representing a transducer finger pair as two infinite coplanar parallel strips [26]. From there, the capacitance of a single pair of electrode fingers can be derived and then the total capacitance can be calculated based on the number of finger pairs. The derivation will be done in free space.

Figure 2.6 shows a single finger pair representation. The terms a and b are the widths of the finger and finger gap respectively. The dielectric constant ε_s is that of the substrate and ε_0 is the dielectric constant of the material above the surface which for this example is assumed to be free space. In order to calculate the capacitance of a single pair of electrode fingers the charges (1) below the electrode surface against the crystal, (2) above the electrode surface, and (3) to the side of the electrodes must be evaluated.

The integration for the charges (1) and (2) will start from the edge of the electrode to the center. The charge is then multiplied by a factor of two to account for the symmetry of the other half of the surface. Charge (3) on the side of the electrodes will simply be evaluated as a parallel plate capacitor. Fig. 2.7 shows the boundaries of integration for the problem. The expression $\frac{L}{2}(1-\alpha)$ is to account for IDT geometries that are not uniform, which have a metallization ratio different than 0.5.

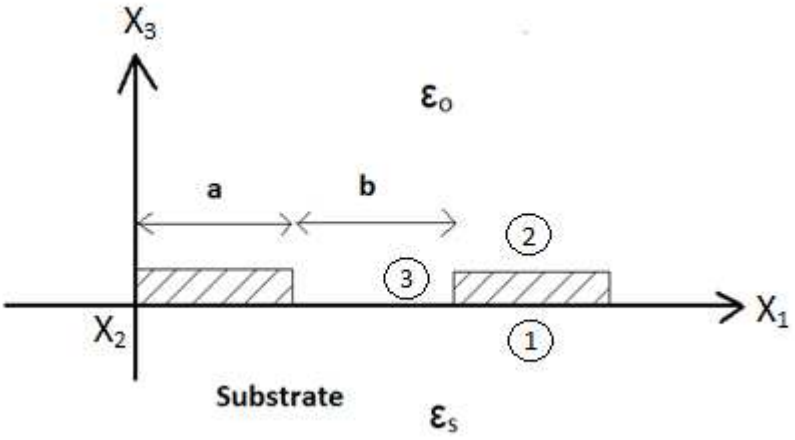

Figure 2.6: IDT finger representation for capacitance calculation

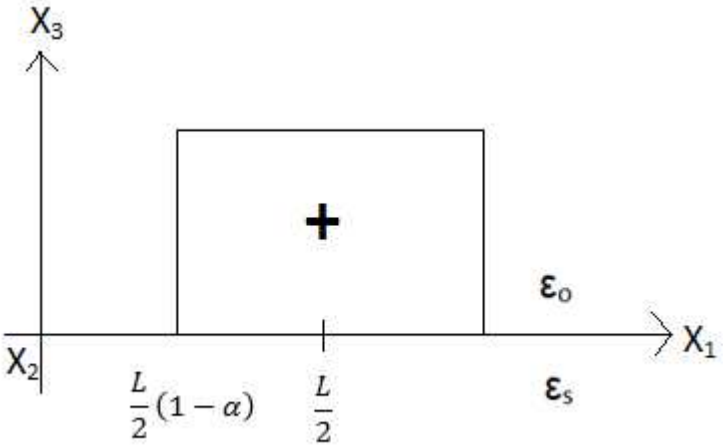

Figure 2.7: Boundary of integration for capacitance

Using Gauss's law, the charge on the electrode surface of the crystal is obtained as

$$Q_{(1)} = 2W \int_{\frac{L}{2}(1-\alpha)}^{\frac{L}{2}} D_3^{(1)}\,(X_3 = 0^-)dX_1 \qquad (2.18)$$

where the expression for the electric displacement $D_3^{(1)}$ is [16]

$$D_3^{(1)} = \varepsilon_s E_3 \frac{K[k]}{K'[k]} \qquad (2.19)$$

$K[k]$ is the complete integral of the first kind to the complementary modulus $k = (1 - r^2)^{1/2}$ where $r = \frac{a}{b}$. This function allows the electric displacement to be integrated over the elliptical path the electric field lines naturally take. Substituting Eq. 2.19 into Eq. 2.18 yields,

$$Q_{(1)} = \frac{1}{2} W \varepsilon_s E_3 L \frac{K[k]}{K'[k]} = \frac{1}{2} W \varepsilon_s V_o \frac{K[k]}{K'[k]} \qquad (2.20)$$

Similarly, the charge on the electrode surface in free space is obtained as

$$Q_{(2)} = 2\mathrm{W} \int_{\frac{L}{2}(1-\alpha)}^{\frac{L}{2}} D_3^{(2)} (X_3 = 0^+) dX_1 \qquad (2.21)$$

where the expression for the electric displacement $D_3^{(2)}$ is [16]

$$D_3^{(2)} = \varepsilon_o E_3 \frac{K[k]}{K'[k]} \qquad (2.22)$$

Substituting equation 2.22 into 2.21 yields,

$$Q_{(2)} = \frac{1}{2} W \varepsilon_0 E_3 L \frac{K[k]}{K'[k]} = \frac{1}{2} W \varepsilon_0 V_o \frac{K[k]}{K'[k]} \qquad (2.23)$$

The capacitance in the form of a parallel plate capacitor for the charges on the side of the electrode can be expressed as

$$C_{(3)} = \frac{\varepsilon_0 t W}{b} \qquad (2.24)$$

where t is the thickness of the electrodes and W is the aperture width of the electrode fingers.

For an applied voltage,V_o, the electrostatic capacitance of a single finger pair in a free space configuration is given by the sum of the contributions of the charges beneath, above, and to the side of the electrodes. The capacitance is given by

$$C_s = \frac{Q_1}{V_o} + \frac{Q_2}{V_o} + \frac{\varepsilon_0 tW}{b} \quad (2.25)$$

The thickness t is negligible in many IDT configurations and as a result, the third term in eq. 2.25 will be omitted. Substituting equations 2.20 and 2.23 into 2.25 and using the expression $C_T = NC_s$ yields the total electrostatic capacitance of the IDT as

$$C_T = \frac{(\varepsilon_o + \varepsilon_s)}{2} NW \frac{K[k]}{K'[k]} \qquad (2.26)$$

2.5 Dielectric Film Loaded Case

In order to use an IDT as a chemical sensing platform, a chemically selective polymer layer must be loaded on top of the transducer. The film will absorb analytes of interest. In addition, the layer can protect the transducer from a conductive liquid layer that may cause a short between the IDT fingers otherwise. In some sensor geometries, a single polymer layer acts as the protective and the chemically selective layer; in other geometries, these layers are separate films.

A dielectric film over the IDT can also help increase the sensitivity of the SH-SAW by acting as an acoustic waveguide. This is done by selecting an overlayer with lower shear wave velocity than the substrate, resulting in a decrease in the penetration

depth and confining more energy to the surface. Trapping more energy to the surface will make the SH-SAW more sensitive to surface perturbations.

As the analytes sorb through the polymer film, changes in the properties of the transduction process can be interpreted for sensing [18]. In order to discuss this theory, a model must be presented that explains how the properties of the transducer change upon adding a thin dielectric layer first. Specifically, the radiation resistance and electrostatic capacitance will be examined. Fig. 2.7 shows the geometry for the problem with the addition of a dielectric film.

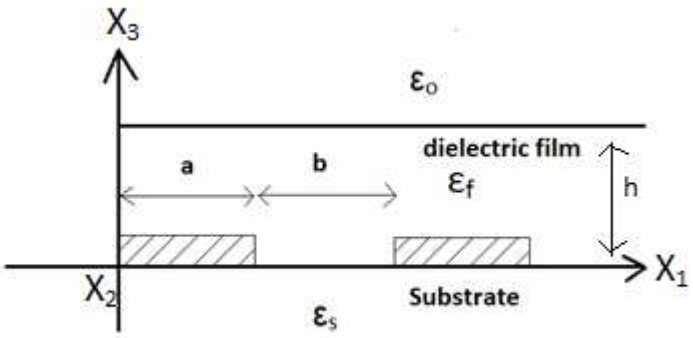

Figure 2.7: Single pair of electrodes loaded with dielectric film

2.5.1 Radiation Conductance

When a thin dielectric layer is deposited on top of the propagating surface, a shear mode can be converted into a Love mode [13]. A Love wave is a shear-horizontal acoustic mode which propagates in a layered structure consisting of a substrate and a guiding layer on top of it. A Love wave can only exist if the shear mode velocity in the

layer is smaller than the shear velocity in the substrate. The guiding layer will slow down the acoustic shear mode at the surface which will decrease the penetration depth and confine more acoustic energy to the surface [28]. The dielectric film can help confine more energy to the surface which will increase the radiation conductance and make the sensor more sensitive to surface perturbations.

How well the guiding layer helps trap energy at the surface also depends on its thickness. Without a film, the acoustic field will deeply penetrate into the bulk. At very small thicknesses of guiding layer, the acoustic fields are "steered" closer towards the surface, resulting in a higher energy density at the surface. With increasing thicknesses, the guiding layer becomes more and more efficient. However, a layer which is too thick will decrease the efficiency of the IDT because too much energy is coupled into the non-piezoelectric waveguide and not through the substrate.

Kovacs et al. have experimented with increasing thicknesses of SiO_2 on ST-quartz and showed the relationship between the electromechanical coupling versus normalized thickness [28]. As the waveguide steers the acoustic wave closer to the surface, the particle velocity projected at the surface increases. This increase in particle velocity causes an increase in the wave energy at the surface, increasing the conductance. For very thick films, the velocity of the SAW is that of the shear velocity of the film which is less than that of the substrate.

The value of k^2 can be obtained by calculating the perturbation of wave velocity Δv due to a change in the electric field boundaries [25]. Specifically, for SAW, a thin

metallization layer is added on top of the transducer and the change in velocity is measured as [25].

$$k^2 = \frac{2|\Delta v|}{v_o} \qquad (2.27)$$

where $\Delta v = v_g - v_m$, with v_g the wave velocity in the guiding layer and v_m the metallized SAW velocity.

Careful consideration needs to be done when deciding on an appropriate film thickness. Too thin a film may not trap enough energy and too thick a film may result in too much energy loss.

The viscoelastic properties of a film will affect the acoustic wave velocity and hence the stress. It is noted that the viscoelastic properties of the film do not affect the capacitance and only the radiation conductance. A higher elastic constant means more stress in the film, resulting in more power associated with the excited wave [29]. This means that the radiation conductance is proportional to the film's elastic constant [29].

2.5.2 Electrostatic Capacitance

The total capacitance of the IDT with an isotropic dielectric film will change depending on the dielectric constant of the film and its thickness. The dielectric constant of the film, ε_f, is proportional to the capacitance contribution from the film. This is easily recognized from basic capacitance theory. At low thicknesses, the dielectric film will cause an initial increase in capacitance. This is due to the fact that more of the electric fields are passing through the film. Thicknesses that go beyond half the wavelength of the IDT start to experience a constant capacitance for increasing film

thicknesses. This indicates a steady-state region and is expected since at large thicknesses, the film starts to behave as a semi-infinite medium. A quantitative expression for the total capacitance of an IDT with a dielectric film is given by [29]

$$C_T = \left\{\left(\varepsilon_s + \varepsilon_f\left[\left(1 - e^{-2\pi h\lambda^{-1}}\right)/\left(1 + e^{-2\pi h\lambda^{-1}}\right)\right]\right)\right\}\frac{K\left[\left(1-r^2\right)^{1/2}\right]}{K[r]}NW \qquad (2.28)$$

where

ε_s = the dielectric constant of the piezoelectric substrate

ε_f = the dielectric constant of the dielectric film

h = the electrode thickness

λ = the transducer wavelength

N = number of electrode pairs

W = the aperture width of the transducer

Eq. 2.28 reduces to Eq. 2.29 as the thickness, h, goes to infinity.

$$C_T = \left(\varepsilon_s + \varepsilon_f\right)\frac{K\left[\left(1-r^2\right)^{1/2}\right]}{K[r]}NW \qquad (2.29)$$

Eq. 2.29 is very similar to Eq. 2.26 for the case of the IDT in free space except that the dielectric of the film is now substituted in. This is because at large thicknesses, the capacitance acts as if the dielectric film is semi-infinite [29].

Figures 2.8 and 2.9 illustrate typical capacitance curves for both $LiTaO_3$ and quartz with varying thicknesses of dielectric films. Because $LiTaO_3$ has a much higher dielectric constant than quartz, the increase in capacitance is much smaller for thicker films. This is because more electric fields are penetrating through the substrate and not the film, which is a great advantage for sensing in liquid environments. The higher the dielectric of the film the greater the change in capacitance is from Eq. 2.29. A liquid

layer will have a high dielectric constant that can absorbed into the dielectric film, increasing the film's dielectric constant.

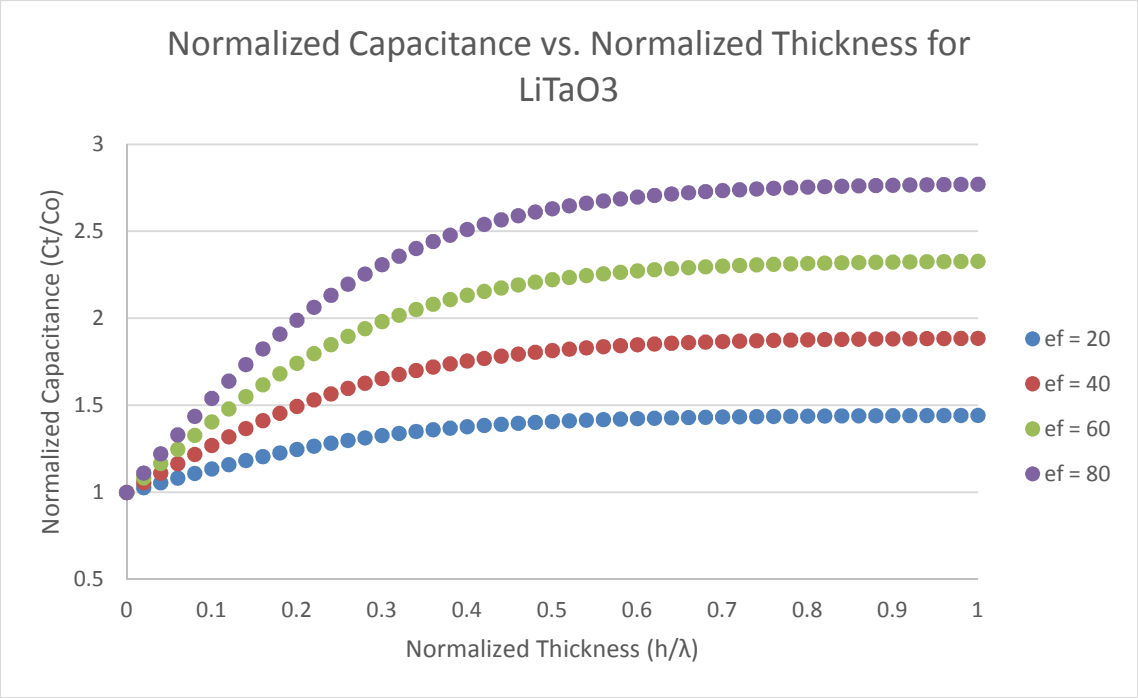

Figure 2.8: Normalized capacitance vs normalized thickness on $LiTaO_3$ substrate, $\varepsilon_s=43\varepsilon_o$ [31]

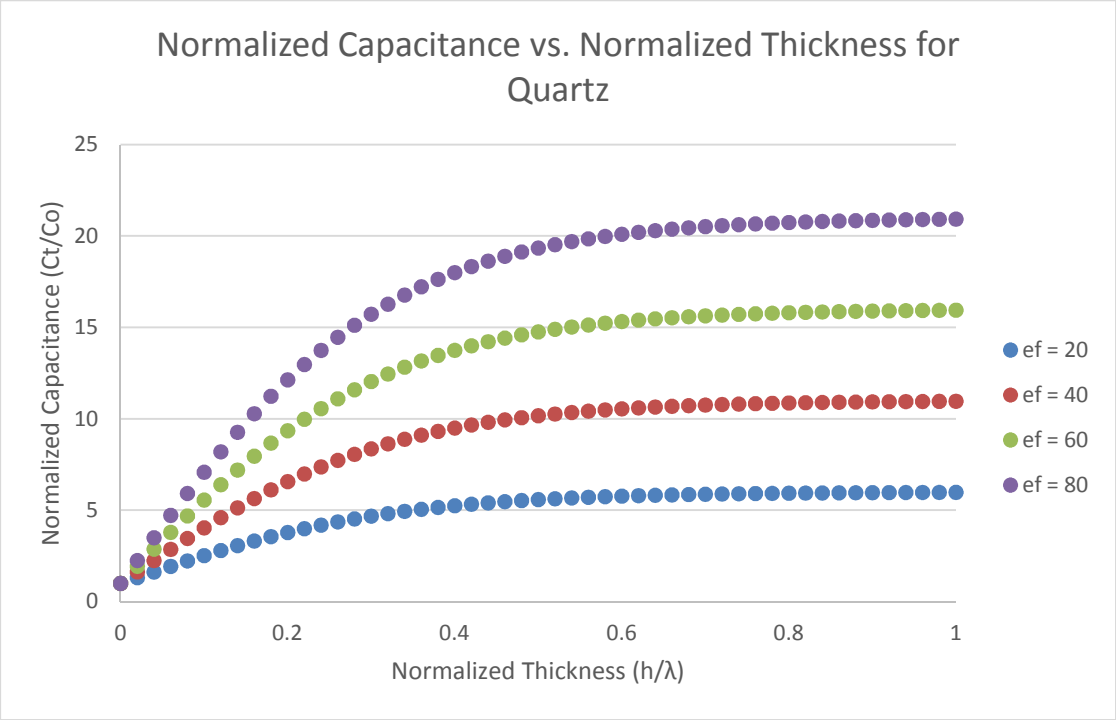

Figure 2.9: Normalized capacitance vs normalized thickness on quartz substrate, $\varepsilon_s=4\varepsilon_o$ [39]

2.6 Case of IDT and Dielectric Film in an Aqueous Solution Case

The modeling of the IDT and dielectric film loaded case assumes that there is free space above the film. When the free space layer is replaced with a liquid layer major changes to the radiation resistance and capacitance occur. Properties of the liquid such as the density and viscosity will affect the IDT parameters.

In order to do liquid sensing a protective dielectric layer is a necessity or else the acoustic wave is considerably damped due to the viscous properties of the liquid. The aqueous solution will be absorbed into the film changing the properties of the film. An aqueous solution will typically have a large dielectric constant and will decrease the electric displacement in the substrate, reducing the acoustic wave energy generated. If

the liquid medium is conductive it can short out the electric fields between the IDT fingers. The velocity of the wave is slowed by the viscous drag of the liquid similar to that of mass loading. Power loss from the wave also occurs due to the viscous medium not moving in phase with the substrate.

2.7 Analyte Absorption and Sensing

As analytes sorb through the polymer film, changes in the polymer's properties will occur resulting in changes in the radiation conductance and capacitance. The changes in film's properties are of two categories: mechanical and electrical. Mechanical properties of interest in this work are mass loading and viscoelastic changes. The electrical property is the dielectric constant. It is noted that the radiation conductance, *G*, is affected by both the mechanical properties and electrical properties while the capacitance, *C*, is only affected by the electrical properties, as indicated by the equations shown below [29].

$$\Delta G = f(\Delta m, \Delta c, \Delta \varepsilon) \qquad (2.30)$$

$$\Delta C = f(\Delta \varepsilon) \qquad (2.31)$$

2.8 Equivalent Circuit Model for Sensing

Figure 2.10 shows the circuit model for an IDT with analyte absorption into the dielectric film in an aqueous environment. The reference conductance G_{ref} is expressed as $G_{ref} = G_o + \Delta G_f + \Delta G_w$ where G_o is the initial conductance of the IDT in the free space case, ΔG_f is the change in resistance from applying a dielectric film, and ΔG_w is the change in resistance from liquid damping. The reference capacitance C_{ref} is expressed as

$C_{ref} = C_o + \Delta C_f + \Delta C_w$ where C_o is the initial capacitance from the free space case, ΔC_f is the change in capacitance from a dielectric film, and ΔC_w is the change in capacitance from liquid damping.

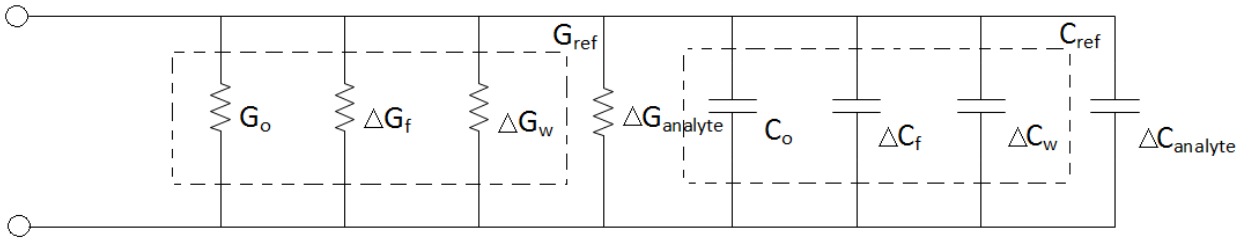

Figure 2.10: Circuit model for IDT with analyte absorption into the dielectric film in an aqueous environment

For chemical sensing, the change in the radiation conductance and capacitance measured needs to be due to the analyte absorption only. Because of this, a differential measurement is needed to isolate the quantities $\Delta G_{analyte}$ and $\Delta C_{analyte}$, the changes in radiation conductance and capacitance from analyte absorption alone respectively. This is performed using a reference IDT that is not exposed to the analytes. The reference values for the radiation conductance and capacitance can be used to make the differential measurement for $\Delta G_{analyte}$ and $\Delta C_{analyte}$ by

$$\Delta G_{analyte} = G_{measured} - G_{ref} \qquad (2.32)$$

$$\Delta C_{analyte} = C_{measured} - C_{ref} \qquad (2.33)$$

2.9 Radiation Resistance

In practice, one would rather measure radiation resistance changes as opposed to radiation conductance changes. An expression for the radiation resistance can be derived from the admittance equation, Eq. 2.9, at the resonant frequency. At the resonance frequency, the radiation susceptance, $B_a(f)$, is zero. Converting the admittance into impedance yields

$$Z = Y^{-1} = \frac{1}{G_a + j\omega C_T} = \frac{G_a - j\omega C_T}{G_a^2 + \omega^2 C_T^2} \qquad (2.34)$$

The real component of the impedance is equal to the radiation resistance, R_a, and is given by from Eq. 2.34 as

$$R_a = Re\{Z\} = \frac{G_a}{G_a^2 + \omega^2 C_T^2} \qquad (2.35)$$

Equation 2.35 shows the equation for the radiation resistance. An expression for the radiation reactance is not necessary since this work will involve working at or around the resonant frequency, in which the acoustic reactance is zero. For either weak coupling materials where the electromechanical coupling coefficient is very small or for materials with a high dielectric constant, which is true for $LiTaO_3$, $G_a^2 \ll \omega^2 C_T^2$ and equation 2.35 can be rewritten as

$$R_a = \frac{G_a}{\omega^2 C_T^2} \qquad (2.36)$$

3. EXPERIMENTAL METHODS AND PROCEDURES

This chapter will discuss the experimental methods used in the detection of OPs. Detailed procedures of how the polymer coatings (PECH, BPA-HMTS) were fabricated and the analyte samples (parathion, parathion-methyl, paraoxon) were prepared will be given. This work is a continuation of work done by previous students in the Microsensors Research Lab at Marquette University [18,37]. Brief descriptions of the instruments and experimental set up used will be discussed.

3.1 Materials and Instruments

3.1.1 IDT

The IDT used in this work is fabricated on a 36 degree-rotated Y-cut X-propagation lithium tantalate (36º YX-$LiTaO_3$) crystal. The crystal supports a shear-horizontal surface acoustic wave. The transducer has a wavelength of 40μm (λ=40μm), an aperture of 2mm (W=2mm), and has 45 finger pairs (N=45) [30]. The device resonates at about 105 MHz in air. This is where the maximum radiation resistance occurs. The piezoelectric coupling coefficient and dielectric constant of $LiTaO_3$ is 0.44 ($k^2 = 0.044$) and $43\varepsilon_o$ ($\varepsilon_s = 43\varepsilon_o$) respectively [31].

The transducer uses a split-finger geometry, meaning the sign of the electric potential of the fingers will switch every two fingers and not alternately. A picture of this geometry is shown in the Appendix. This geometry is known to reduce signal reflections between the fingers, thus reducing signal distortions due to triple transit echoes [32]. More accurate approximations for the capacitance can be found in literature [13] for this

transducer geometry but will not be discussed since the radiation resistance and frequency shift will be the key parameters of interest.

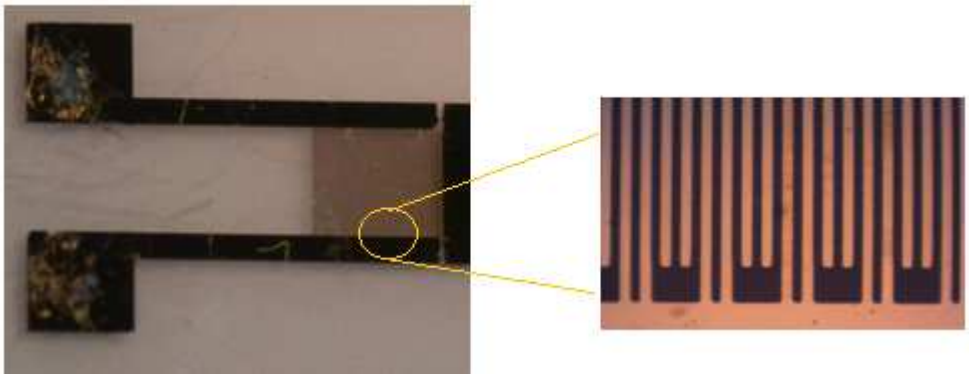

Figure 3.1: IDT and microscopic picture of IDT fingers

3.1.2 Organophosphates

The OPs of interest for this work are parathion, parathion-methyl, and paraoxon. All three of which are known to be toxic to humans.

Parathion and parathion-methyl were first developed as insecticides but now their uses have been severely restricted since the EPA has considered them to be possible human carcinogens. In their pure forms they are white crystalline solids; however, parathion is usually transported in a liquid form [33,34]. Parathion in liquid form and parathion-methyl in crystalline form are obtained from Sigma Aldrich. Parathion-methyl is dissolved in methanol as an extra step before used to make the analyte samples. Parathion has a molecular weight of 291.26 mol/g and its molecular structure can be referred to in Fig. 3.1(a) [33]. Parathion-methyl has a molecular weight of 263.21 mol/g and its molecular structure can be referred to in Fig. 3.1(b) [34].

Paraoxon is the active form of parathion when broken down. It is considerably more toxic and harmful [35]. Paraoxon is also supplied to us from Sigma Aldrich in a liquid form. The molecular structure of paraoxon is shown in Fig. 3.2 and has a molecular weight of 275.2 mol/g [36].

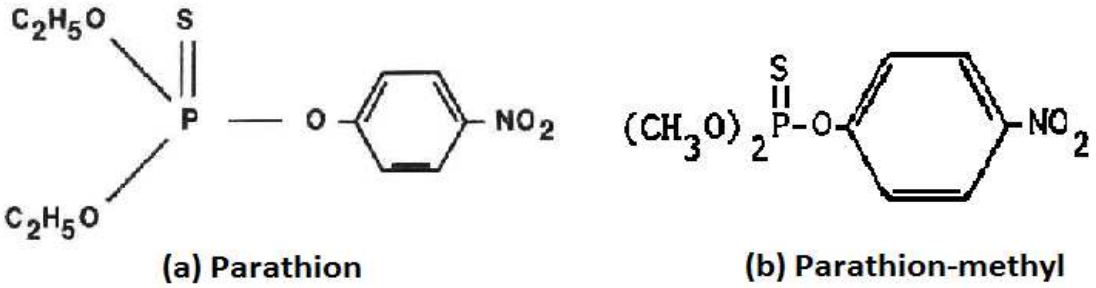

Figure 3.2: Molecular structures of (a) parathion and (b) parathion-methyl [6,7]

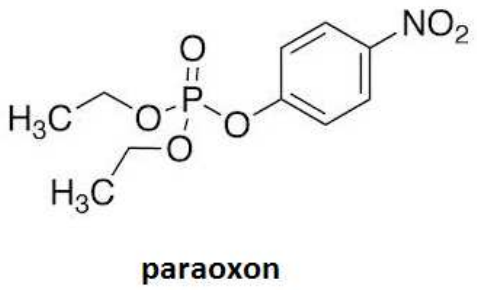

Figure 3.3: Molecular structure of paraoxon [8]

3.1.3 Polymers

The two polymer layers that will be used for sensing OPs are 2,2'-diallylbisphenol A – 1,1,3,3,5,5-hexamethyltrisiloxane (BPA-HMTS) and polyepichlorohydrin (PECH). PECH is purchased from Sigma Aldrich and diluted in

chloroform. BPA and HMTS are bought from Sigma Aldrich but synthesized here at Marquette University to make BPA-HMTS using a hydrosilylation reaction [36,37]. The HMTS group serves as the backbone for analyte absorption. The motive for synthesizing BPA-HMTS was to reduce the response times that were observed with other films such as PECH. The steps for making these polymers solutions are described in Section 3.2.3 [18,36].

3.1.4 Spin Coater

In order to ensure a smooth and even polymer distribution on top of the IDT, a Specialty Coating Systems (SCS) Model P6024 spin coater was used. The process involves depositing a few drops of the polymer on top of the device and spinning the device at a high spin speed to ensure the device is evenly coated. Factors that affect the thickness of the film are: the spin speed, ramp time, hold time, polymer solution viscosity, and percent weight of polymer solution [38]. The spin coater was used to produce film thicknesses of 0.50μm and 0.75μm for PECH and BPA-HMTS.

3.1.5 Ellipsometer

The Gaertner Scientific L2WLSE544 Stokes Ellipsometer [39] was used to measure polymer film thicknesses. This was used to ensure that a device was coated properly before testing. The ellipsometer measures thickness by a laser beam reflected off the surface of the polymer at a low angle of incidence. The beam would reflect both at the surface and at the bottom of the film and the phase shift would be measured as the beam passed through the output detector. This phase shift is used to calculate the thickness of the polymer. Two lasers of different wavelengths were used to ensure

accurate thickness readings. The wavelengths of the lasers are 543.5 (green) and 632.8 (red) nm.

3.1.6 Flow Cell

The IDT device is tested in a flow cell. The flow cell allows for the aqueous solutions to come into contact with the surface of the IDT. The flow cell was designed by F. Josse from Marquette University and R.W. Cernosek [40] from Sandia National Laboratories and is used worldwide in various research labs. The flow cell comprises of 3 separate pieces. The bottom piece contains a recessed area for the SH-SAW device to fit in. The middle piece contains contact pins which provide a connection between the device and network analyzer. The top piece allows for inlet and outlet of the aqueous solution. A gasket is used to ensure a tight seal so that the solution can be pumped. The top piece is made of polycarbonate so that it does not react with the aqueous solution. The bottom and middle pieces are made out of brass to shield any electromagnetic interference away from the device. Figure 3.3 shows the parts of the flow cell.

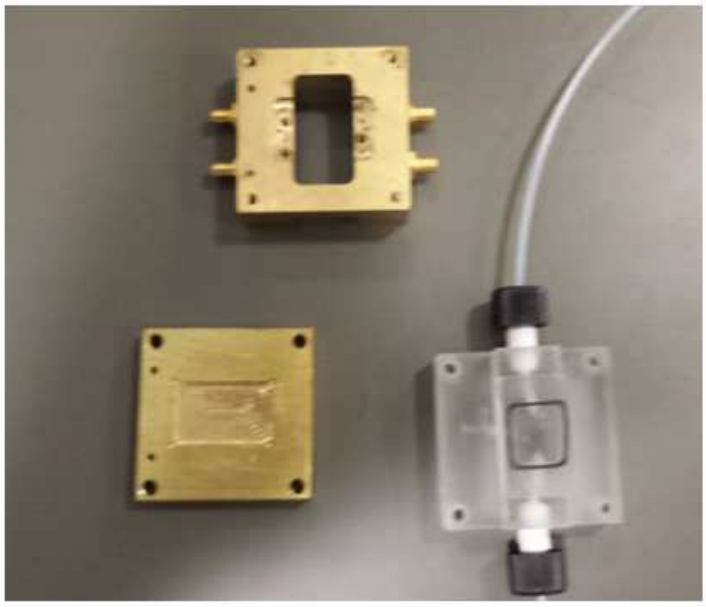

Figure 3.4: Parts of flow cell: bottom piece (bottom left), top piece (bottom right), middle piece (top)

3.1.7 Pump

An Ismatec RS232 peristaltic pump was used to pump the reference and analyte solutions into the flow cell. These special pumps allow the liquid to be pumped at a very stable and constant velocity. This is to reduce any unwanted noise from turbulence. The pump has a start/stop function for switching analyte solutions. The pump velocity for this experiment was kept at 12 μl/s.

3.1.8 Network Analyzer

The HP 8753C Network Analyzer was used for measuring the sensor parameters. The network analyzer is capable of characterizing a device by performing a frequency sweep and measuring various parameters as a function of frequency. For this work, the

radiation resistance of the device was measured over a set frequency range. The network analyzer has the ability to track specified resistance values and monitor the change in frequency. Also, the network analyzer can track the change in resistance value at a specified frequency. Both of these functions were used on the network analyzer to track the change in radiation resistance and frequency shift.

3.2 Experimental Procedures

This section will describe all the procedural steps taken to synthesis the polymers and to produce the OP analyte solutions for detection. A description and diagram of the experimental set up will also be shown.

3.2.1 Experimental Setup

A peristaltic pump is used to pump the analyte solution through the flow cell for detection. The solution then exits the flow cell into a waste container. The network analyzer is connected to the flow cell's outputs via SMA cords. Measurements are performed using the network analyzer and transferred to a personal computer with Labview software for storage of data over time. Fig. 3.4 shows a process flow diagram of the setup. The samples and flow cell are kept in a cooler box to prevent any temperature changes from the outside environment. LiTaO3 has a relatively large temperature coefficient of delay and so fluctuations in the ambient temperature can affect the measurement accuracy [31].

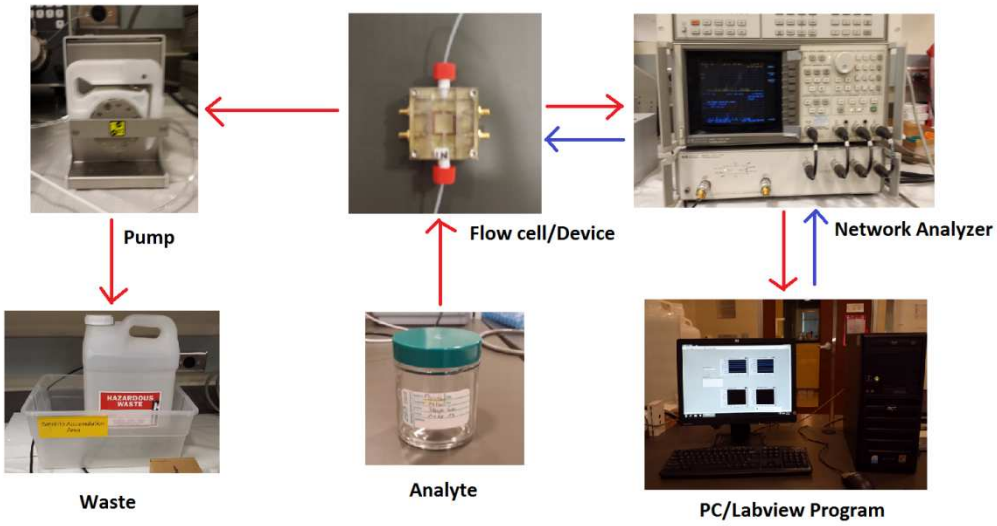

Figure 3.5: Experimental setup flow diagram

3.2.2 SH-SAW Preparation

The SH-SAW device goes through several preparation steps before being used for testing. First, the edges of the device are filed using sandpaper to create a rough surface. The rough edges will scatter the acoustic waves at the ends of the device so that none are reflected back to the transducer. Since the IDT is of interest and not the delay line, small grooves are etched with a fine blade on the delay line surface. This mitigates any triple transit signals from interfering with the wave from the IDT [18]. Before coating, the device is washed using trichloroethylene, chloroform, acetone, and 2-propanol in an ultrasonic bath for 3 minutes in that order respectively. The device is washed with DI water in between cleaning solutions and then dried with nitrogen gas for the last step.

The cleaning process ensures adequate adhesion of the polymer layer onto the surface. Once coated, the bottom layer of the device is covered in electrical tape to

absorb any bulk waves associated with the IDT. The bulk waves are absorbed into the tape layer and do not reflect back to the surface. Overtime, the contacts from the flow cell can scratch the IDT contact pads. Small amounts of silver paint are placed on the IDT contacts to ensure good contact between the device and flow cell if the contacts are scratched or damaged.

3.2.3 Polymer Synthesis

After the SH-SAW device is prepared sufficiently, it is then coated. The polymers for both PECH and BPA-HMTS are used to make the polymer solutions. PECH is bought from Sigma Aldrich and is used as received. BPA-HMTS however is synthesized at Marquette University using BPA and HMTS [36]. The preparation for the PECH solution is done using the following steps [36,37].

1. Determine the % wt. needed by using Eq. 3.1
2. Place a clean 20mL vial on the scale and tare.
3. Add the mass of PECH calculated from Eq. 3.1 into the vial.
4. Add the needed amount of chloroform to achieve the % wt. from Eq. 3.1
5. Add a stir bar, cap, and seal the vial using Teflon tape
6. Stir the polymer at 1000rpm at 120ºC for 2 hours and then with no heat for another 22 hours.

$$\%wt. = \frac{Mass\ of\ BPAHMTS(or\ PECH)}{Mass\ of\ Chloroform} x100 \qquad \text{(Eq. 3.1)}$$

Synthesis of the BPA-HMTS is done at Marquette University [36]. The steps in synthesizing the polymer are listed below [36,37].

1. Turn on Corning (420D) hotplate and set plate temperature to 250 °C to heat oil bath (100-110 °C).
2. Add 10 mL of toluene into 40 mL vial and reset scale to zero.
3. Add (0.882 g, 0.00286 mol) of BPA (Mw = 308.41 g/mol).
4. Stir mixture on stir plate for about 5 min at 400 rpm until a homogeneous mixture is obtained.
5. Add 10 mL of toluene and reset scale to zero.
6. Add (0.566g, 0.00271 mol) of HMTS (Mw = 208.48 g/mol) to give a mole ratio for reacting functional groups, r = [SiH]/[CH2=CH], of 0.95.
7. Stir for about a 1 min and monitor the presence of the Si-H (2125 cm-1) group by FTIR (see Figure 4.5a).
8. Set scale to zero and add two drops (~ 0.02 g) of Pt-DVTMDS.
9. Stir the solution at 400 rpm in the oil bath (110-115 °C) for 20 minutes.
10. Monitor the disappearance of the Si-H (2125 cm-1) group by FTIR (see Figure 4.5b).
11. Add 0.17 g (for a total of 0.736 g, 0.00353 mol, r = 1.23) of HMTS to the reaction mixture and stir for 20 minutes.
12. Monitor the presence of excess Si-H by FTIR spectra (see Figure 4.5c)
13. Add five drops (~ 0.058 g) of the catalyst to terminate the polymer with vinyl groups.
14. Repeat steps 1-13 for another vial.

15. Transfer samples into three-neck round-bottom flask.

16. Polymerize using a reflux set-up in an oil bath at 100-110 °C for 2 hours while stirring.
17. Monitor the disappearance of the Si-H (2125 cm-1) group by FTIR.
18. Add activated carbon to mixture and stir in oil bath for 30 minutes to remove the catalyst.
19. Filter solution to remove activated carbon. Finest particle size filter paper is recommended. Filter at least three times.
20. Remove solvent by rotary evaporation. Care must be taken to not perform rotary evaporation for too long, otherwise some of the sample may be lost.
21. Transfer to a watch glass and heat under vacuum at 60 °C for 36 hours to remove residual solvent.
22. Monitor the disappearance of the Si-H (2125 cm-1) group by FTIR (see Figure 4.5d). Note that the amplitude associated with O-H stretching mode is larger because the solvent has been removed.

Once the polymer is finished, the polymer is ready to be made into a solution which is prepared similarly to PECH by the steps below [36,37].

1. Determine the % wt. needed by using Eq. 3.1
2. Place a clean 20mL vial on the scale and tare.
3. Add the mass of BPA-HMTS calculated from Eq. 3.1 into the vial.
4. Add the needed amount of chloroform to achieve the % wt. from Eq. 3.1
5. Add a stir bar, cap, and seal the vial using parafilm
6. Stir the polymer at 1000rpm at room temperature for 1 hour.

The polymer is coated onto the device using a spin coater. Table 3.1 shows the %wt, spin speed and hold time needed to obtain the specific polymer thicknesses.

Polymer	% wt.	Spin Speed (rpm)	Hold Time (s)	Average film thickness (µm)
BPA-HMTS	4.60	3000	30s	0.50
BPA-HMTS	8.00	4000	30s	0.75
PECH	2.10	3500	30s	0.50
PECH	2.10	2500	30s	0.75

Table 3.1: Spin coater parameters and polymer %wt. to achieve desired film thicknesses

3.2.4 Phosphate Buffer Solution

Phosphate buffer solution (PBS) is used for preparing the reference solution and analyte samples. This is to ensure a constant pH level for the OPs. The preparation of 0.1M PBS solution has a pH level of 6.2 and is done by the following steps [36,37].

a) Monobasic Preparation
    1. Measure 1.361g of KH_2PO_4 into a 1000 mL flask
    2. Add and fill the 1000 mL flask with degassed DI water

b) Dibasic Preparation
    1. Measure 1.742g of K_2HPO_4 into a 1000 mL flask
    2. Add and fill the 1000 mL flask with degassed DI water

c) Combine solutions
    1. In a 2000 mL flask, add 173.6 mL of the monobasic solution
    2. Combine with 26.4 mL of dibasic solution
    3. Fill remaining flask with degassed DI water and mix

3.2.5 Reference Solution

1. Measure 960 mL of PBS into a 1000 mL flask
2. Add 1.11 mL of methanol
3. Add stir bar and seal with parafilm
4. Stir at 1000 rpm for 1 hour

3.2.6 Concentrated Analyte Solution

1. In a 20 mL vial, add either 25.8uL, 25.7uL, or 24.1uL of parathion, paraoxon, or parathion-methyl stock solutions respectively.
2. Add 3mL of methanol.
3. Add stir bar, cap, and seal
4. Mix at 1000 rpm for 15 minutes
5. Store at a temperature of 2-5ºC

3.2.7 Analyte Solutions

1. In a 120 mL jar, measure 120 mL of PBS.
2. Add 140uL of the concentrated analyte solution from the fridge. (makes 12 mg/L concentration)
3. Add stir bar, cap, and seal.
4. Stir at 600rpm for 2 hours.
5. Using the dilution chart (Table 3.2), dilute the 12 mg/L analyte sample with reference solution into 0.5, 1.0, 1.5, 2.0, 2.5, and 3.0 mg/L concentrations.

6. Mix all concentration samples for 20 minutes.

Reference Solution (mL)	Analyte Solution (mL)	Concentration (mg/L)
121	5	0.5
116	10	1.0
111	15	1.5
106	20	2.0
101	25	2.5
96	30	3.0

Table 3.2: Dilution chart for making analyte concentrations

3.3 Data Acquisition and Processing

This section explains how the network analyzer is used to make the sensor measurements and how the data is collected and post-processed.

3.3.1 Data Collection

The network analyzer measures the sensor parameters of interest, radiation resistance and frequency. The data is then collected and logged using a Labview program. The program collects data points every 5 seconds from the network analyzer. This allows measurements over time to be collected so that changes in radiation resistance and frequency can be monitored as analyte solutions are pumped into the flow cell.

The network analyzer can display and measure two channels simultaneously. Both channels will display the radiation resistance over a frequency interval which includes the resonant frequency. The marker on the first channel will be set at a fixed

frequency and the radiation resistance will be measured at that frequency every 5 seconds. The marker on the second channel will be set at a fixed radiation resistance value so that the frequency can be measured every 5 seconds at a constant resistance. The location of the markers will be set approximately at the 3dB point to the left of the resonant frequency. Points near the resonant frequency experience large noise levels, so the 3dB point is used instead.

3.3.2 Data Processing

The system experiences a slight drift which causes the radiation resistance to gradually decrease over time, so the baseline is gradually changing [42]. In order to compensate for this drift, a baseline correction is performed after each experiment. The baseline correction will keep the baselines between each sample concentration constant so that it is easier to see the difference in signal change between each sample. Also, the baseline is normalized to zero to see the relative change. Figs. 3.5 and 3.6 show an example of how the raw data is baseline corrected from an experiment using 0.50μm thick BPA-HMTS and parathion.

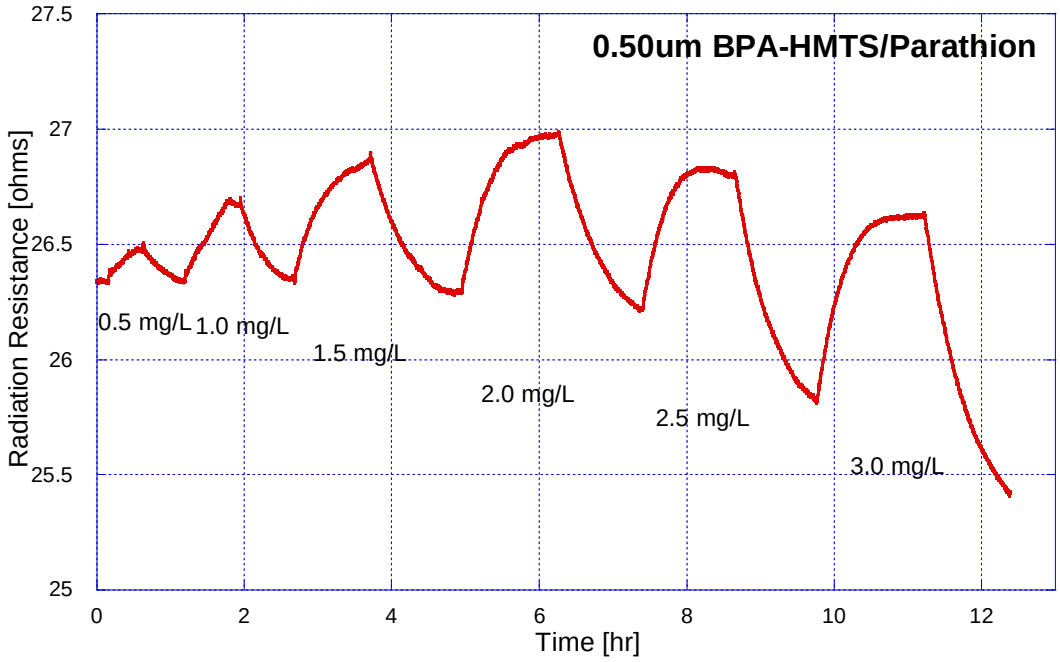

Figure 3.6: Raw data taken from experiment with 0.50µm BPA-HMTS/parathion

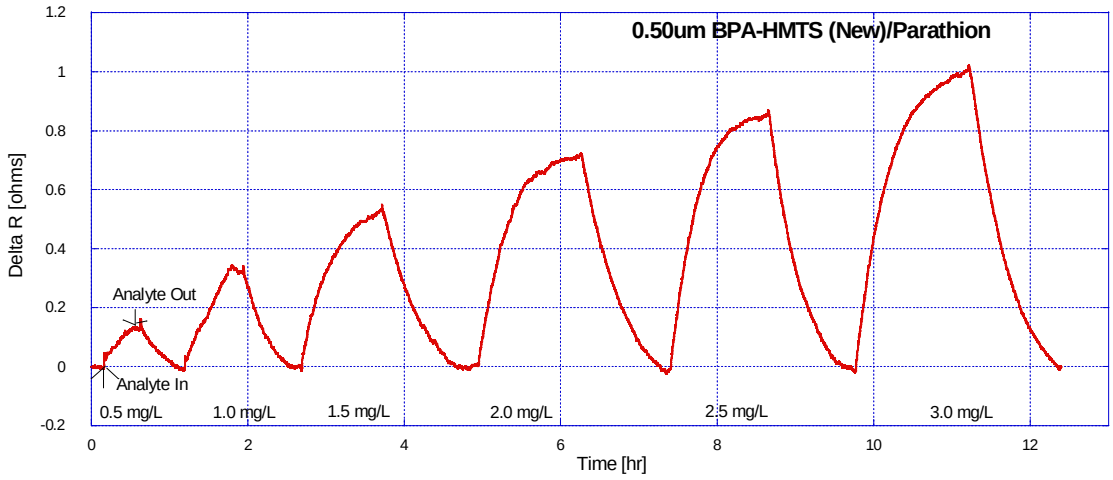

Figure 3.7: Fig. 3.5 after baseline correction

4. RESULTS AND SENSOR ANALYSIS

4.1 Introduction

The theory of the single IDT sensor has been discussed in Chapter 2. The electrostatic capacitance, C_T, and radiation resistance, R_a, from the single IDT circuit model are dependent on the piezoelectric material, transducer geometry, and adjacent medium. When a selective film is coated onto the IDT and used for sensing, changes in the film properties will occur. These changes in the film properties will be reflected in a corresponding change in the IDT circuit model. These changes in the IDT characteristics are calculated and related to the analyte concentration for chemical sensing.

In this chapter, experimental data from the single IDT sensor will be presented and discussed. First, the response of the IDT sensor will be evaluated in air. Then the coated IDT case will be looked at in air and water. Lastly, the performance of the single IDT device coated with two different partially selective films (BPA-HMTS and PECH) for the detection of three organophosphates (Parathion, Parathion-methyl, Paraoxon) in liquid will be investigated.

4.2 Response of the Sensor Device in Air

Measurements of the IDT are first performed in air. This is a close approximation to the free space case as discussed in the theory of chapter 2. Figures 4.1 and 4.2 show the radiation resistance and reactance for a split-finger transducer, on a 36° YX-$LiTaO_3$

substrate with number of finger pairs, $N = 45$, aperture width, $W = 2mm$, and wavelength, $\lambda = 40\mu m$, measured in air case [43].

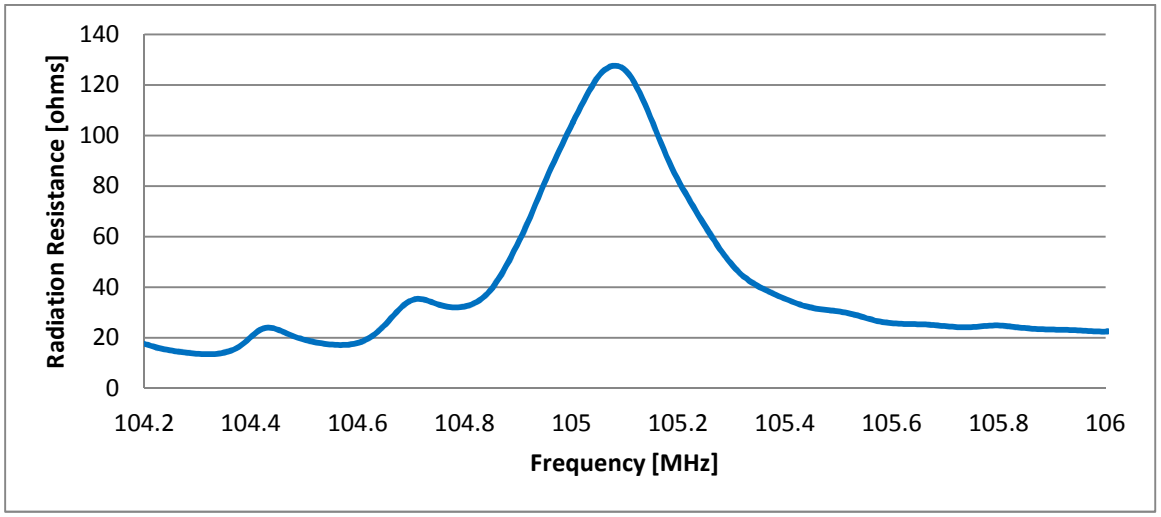

Figure 4.1: Radiation resistance for a split-finger transducer with number of finger pairs, N=45, IDT aperture, W=2mm, and wavelength, λ=40μm, on 36 degree rotated YX-$LiTaO_3$ measured in air.

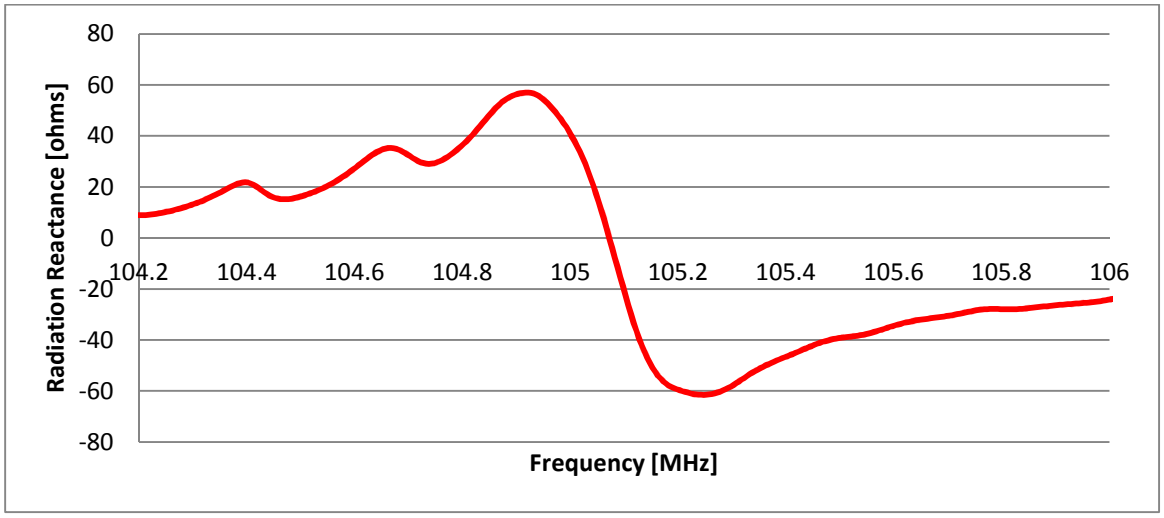

Figure 4.2: Radiation reactance for a split-finger transducer with number of finger pairs, N=45, IDT aperture, W=2mm, and wavelength, λ=40μm, on 36 degree rotated YX-$LiTaO_3$ measured in air.

The resonant frequency can be evaluated at the peak radiation resistance value. From Figure 4.1, the IDT has a peak radiation resistance of 127.6Ω at the resonant frequency of 105.08 MHz. The total capacitance of the IDT, C_T, can further be evaluated from the reactance value at the resonant frequency. At the resonant frequency, the acoustic reactance, X_a, is zero and so the reactance at that frequency is due to the capacitance from the IDT. The capacitance can be calculated from the reactance by the circuit equation $X_c = -\frac{1}{\omega_o C_T}$. From Figure 4.2 the reactance at the resonant frequency is -9.58Ω which correlates to a capacitance of $C_T = 158.1$pF. The electrostatic capacitance is a measure of the charges stored on the IDT at the film-substrate interface and the radiation resistance (or radiation conductance) is a measure of the input electrical power converted into acoustic power.

The plots of the radiation resistance and reactance from Figures 4.1 and 4.2 have good agreement to the equations for the conductance and susceptance from Equations 2.14 and 2.15. We can measure radiation resistance instead of radiation conductance because the two are proportional to each other. It can also be seen that as the frequency deviates from the resonant frequency, the radiation resistance begins to decrease. This is due to the fact that an acoustic reactance is now arising which decreases the power in the acoustic wave.

From Figures 4.1 and 4.2, the peak radiation resistance is much more stable than the radiation reactance at the resonant frequency, which is shown to be near asymptotical. This yields more stable measurements when measuring the radiation resistance as opposed to the reactance. Any error in measuring the resonant frequency will greatly

influence the capacitance value whereas only moderately influencing the radiation resistance.

4.3 Coated IDT Response

For a particular substrate and IDT geometry, the electrical properties of the equivalent circuit model are shown to depend on the adjacent medium above. In the previous section, the medium the transducer was measured under was air which has a dielectric constant of approximately ε_o. In this section the medium will be replaced by a film with dielectric constant ε_f and thickness h. Introducing a film will change the quantities of R_a and C_T as discussed in Chapter 2. Further changes in the film properties from viscoelastic changes and mass loading due to analyte absorption are exploited for chemical sensing [12]. In this section, first changes in the thickness of a polymer will be looked at in air to see how both R_a and C_T change and then a film layer will be immersed in water to further see how R_a and C_T change.

4.3.1 Effect of Variation of Film Thickness

Figure 4.3 shows the radiation resistance for the same IDT as in Figures 4.1 and 4.2 but coated with different thicknesses of PMMA (poly-methyl methacrylate). The thickness values range from 0.22μm to 1.20μm thick. Figure 4.4 shows the change in R_a with respect to the initial uncoated case for the given thicknesses of PMMA.

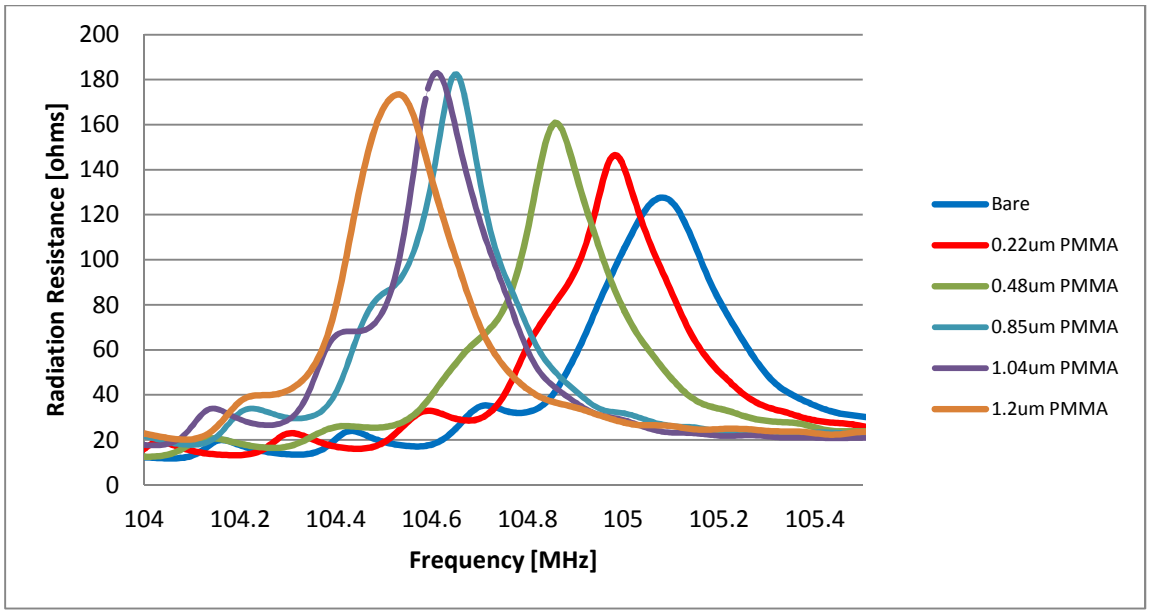

Figure 4.3: Radiation resistance curves for various thicknesses of PMMA

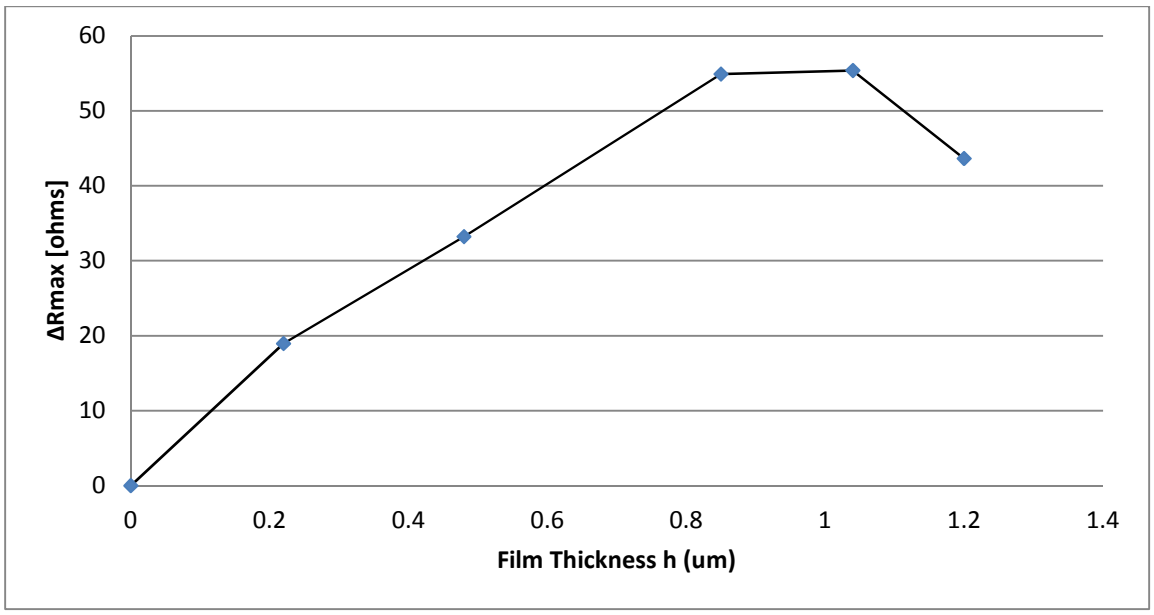

Figure 4.4: Change in the peak radiation resistance due to various thicknesses of PMMA

By first loading a thin dielectric film onto the IDT, initially the radiation resistance begins to increase because the film is guiding the acoustic wave closer to the surface. As the thickness increases, the wave is becoming more efficiently trapped. For

too large film thicknesses, the radiation resistance begins to decrease due to power being driven into the non-piezoelectric film [13]. This can be seen in Figures 4.3 and 4.4 for 1.20μm thick PMMA. At around that thickness, the radiation resistance begins to decrease and is expected to decrease further with increasing thickness.

Figure 4.3 also shows a shift in the resonant frequency for increasing thicknesses of PMMA. Theses shifts are due to mass loading. For a fixed film density and surface area, an increase in the thickness directly correlates to a proportional increase in the mass loaded on top of the IDT. Mass loading perturbs the wave velocity which changes the resonant frequency of the device. This effect is seen in all acoustic-wave modes. A very general description for the relationship between mass-loading, Δm, and frequency shift, Δf_m, for an AW device is given by

$$\Delta f_m = -\kappa S_m \Delta m$$

In which S_m is a device constant which depends on the nature of the piezoelectric substrate, device dimensions, frequency of operation, and acoustic mode. κ is a geometric factor for the fraction of the active device being perturbed. As long as S_m does not depend on film thickness From Equation 4.1, a linear dependence between the added mass and change in frequency is predicted. [12]

Figure 4.5 shows the change in the resonant frequency from the initial air case with respect to increasing thicknesses of PMMA. The data shows good agreement for the linear dependence equation from Equation 4.1. This linear dependence between the frequency shift and added mass only occurs for acoustically thin films. For acoustically thin films, the particle displacement is constant across the film thickness. This is because the entire film is moving in phase with the wave. If the film is acoustically thick, the

upper portion of the film tends to lag behind the bottom substrate/film portion of the film. This deformation results in a non-uniform displacement across the film. Increasing the thickness to the regime of acoustically thick films will result in an exponential decrease in the resonant frequency as opposed to a linear decrease with the acoustically thin film case. [12]

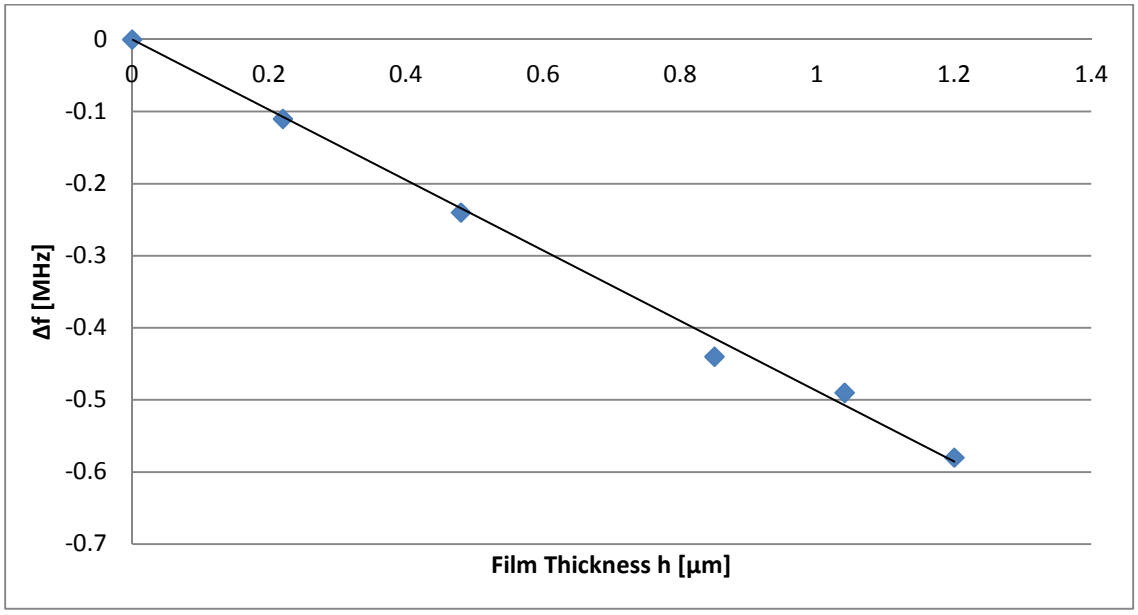

Figure 4.5: Shifts in resonant frequency due to increasing film thicknesses of PMMA

Similarly the reactance plots for each of the PMMA thicknesses are shown in Fig. 4.6. Small bar lines indicate the resonant frequency for each of the thicknesses. Experimentally it is difficult to accurately track the reactance value at the resonant frequency because of the near-vertical nature of the plots around the resonant frequency. A trend towards the increase in capacitance with increased film thickness is observed but the error from the experiment does not permit a more detailed analysis.

The results from Fig. 4.7 do show an increase in capacitance as a film is loaded to the IDT as expected from Chapter 2. However, the data itself is not as consistent as that of the radiation resistance due to the difficulties in tracking the reactance at the resonant frequency. One would expect an initial increase in capacitance from applying a dielectric film and then a small change with increasing thicknesses of the film.

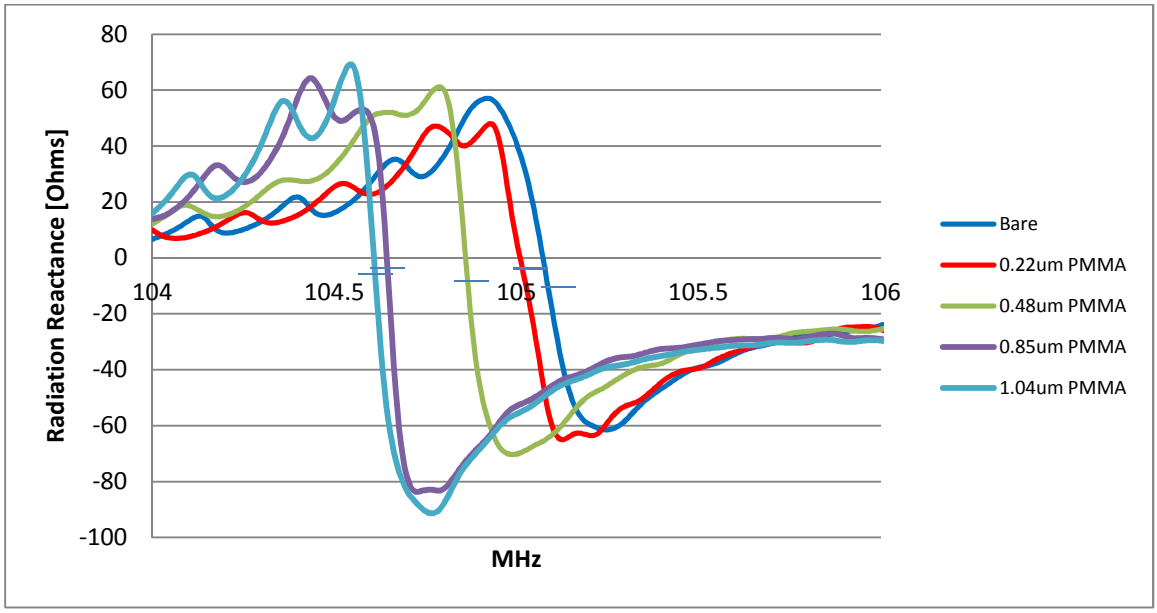

Figure 4.6: Radiation reactance for varying thicknesses of PMMA

4.3.2 Effect of Water Loading

The next case that will be looked at is the water loaded case. This is done by coating the IDT with a dielectric polymer and adding droplets of water on top of the film. The water will absorb into the film and change the radiation resistance and capacitance. The polymer PECH will be used for this case. In order to obtain a reasonable response in

water, a polymer layer must be used to shield the IDT from the water that may otherwise short the IDT fingers.

Figures 4.8 and 4.9 show the radiation resistance and reactance curves for an IDT coated with a 0.65µm PEA film layer in air and subjected to water droplets. Note that a dielectric layer is necessary to get any reasonable measurement in liquid. This is because the liquid may short the IDT fingers if conductive and greatly reduce the electric fields within the substrate due to the high dielectric constant of water. And without a film, the acoustic waves are not being guided to the surface making the device even less efficient. Note that in this experiment, two major factors are contributing to the changes in the radiation resistance and reactance, viscous loading of the water droplets and the change in the dielectric constant of the film due to water absorption.

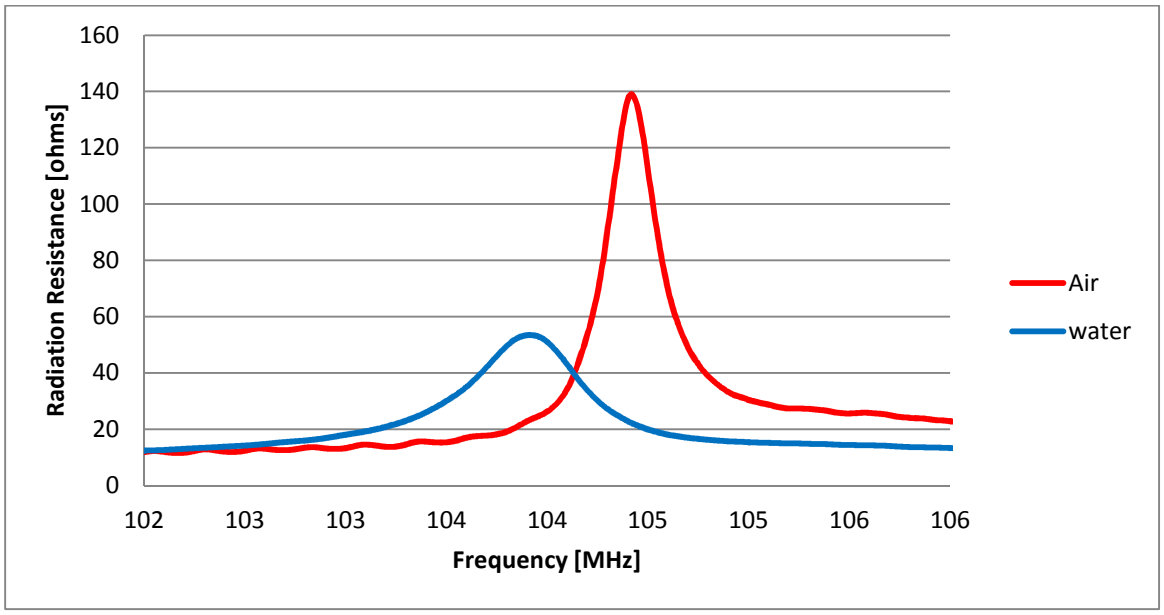

Figure 4.7: Radiation resistance curves measured for an IDT coated with a 0.65µm PEA film in air and with water droplets added

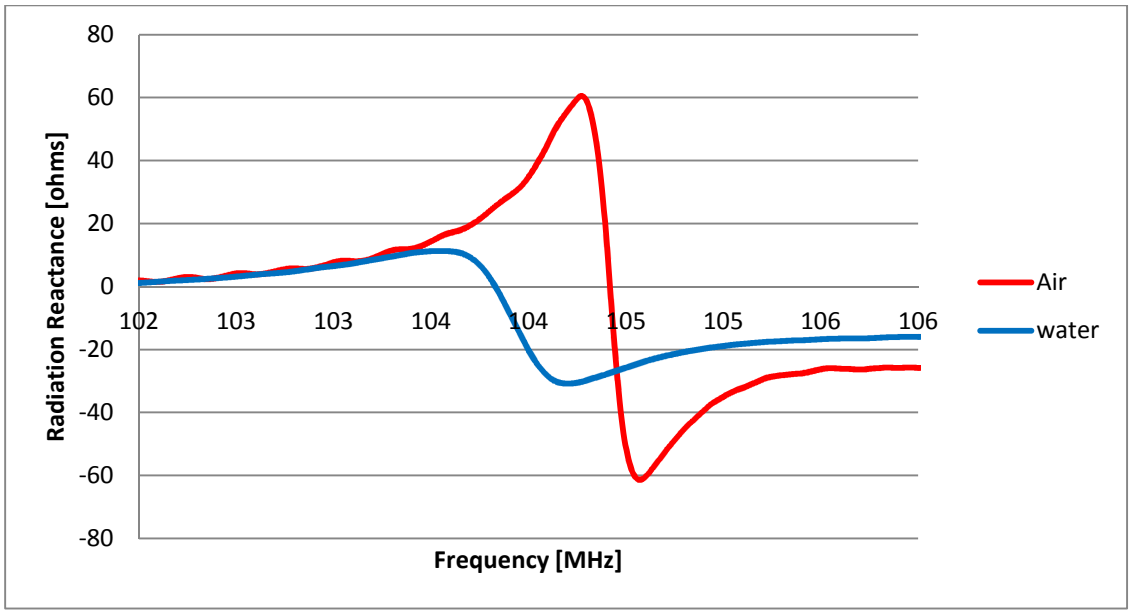

Figure 4.8: Reactance curves measured for an IDT coated with a 0.65µm PEA film in air and with water droplets added

From Fig. 4.8, the radiation resistance shows a large decrease when the film is subjected to water compared to air. This is due to water being in contact with and getting absorbed into the PEA film and increasing the dielectric constant of the film. A film and water layer with a much higher dielectric constant will cause more electric displacement to occur within the film/water layer and not the substrate; thus less electrical energy is being converted into acoustic energy. The difference in resonant frequency is largely due to the mass of the liquid vibrating with the wave and causing it to slow down.

The measured reactance at the resonant frequency for the IDT coated with 0.65µm of PEA is -11.98Ω in air and -7.83Ω in water. The capacitance calculated from these values and the resonant frequencies are 127.3 pF in air and 195.8 pF in water. This increase is due to the increase in the dielectric constant of the film as water absorbs through. The dielectric constant of water is much higher ($80\varepsilon_0$) than that of most

dielectric films ($2 - 4\varepsilon_o$) and so the resultant dielectric constant from the water and film will be much higher.

4.4 Detection of Organophosphates in Aqueous Solutions

The performance of the single IDT sensor will now be looked at for the detection of organophosphates in aqueous solutions. Data for a sensor array will be presented and discussed. The array consists of using two polymer coatings (PECH and BPA-HMTS), at two thicknesses (0.50μm and 0.75μm), and has been used for the detection of three organophosphates (parathion, parathion-methyl, and paraoxon). For each OP measurement, 5-6 different analyte concentrations will be measured ranging from 125ppb to 3ppm. This is to ensure that an accurate sensitivity and limit of detection can be calculated. The performance of the two films will then be evaluated by comparing the sensitivities and limit of detections for the three organophosphates. The selectivity will be discussed by use of a sensor array and visual pattern techniques. Finally, a test on the reproducibility of BPA-HMTS will be presented and discussed.

4.4.1 Sensor Response

The sensor responds when an interaction between the analyte and polymer occurs. As analyte absorbs through the polymer film, a number of properties are changing in the film resulting in a change in the radiation resistance. These properties are mass loading, viscoelastic changes, change in dielectric constant, and change in thickness of the film. The combined change in radiation resistance from all these factors is measured for each analyte concentration for a given test by use of a reference measurement. The reference measurement consists of the polymer film and liquid layer

without introducing analytes. This measurement is used to differentiate the change in the radiation resistance from the analyte absorption alone.

The change in capacitance is not shown for this experiment. The point of interest for this experiment is to study the sensitivity of acoustic waves with respect to surface perturbation. Acoustic waves have been known to be extremely sensitive to surface perturbation and this is exploited when to tracking the change in radiation resistance. In theory one can use this design as a capacitive sensor in which changes in the dielectric constant and thickness of the film can be observed. However, this will lead to lower sensitivity than tracking the radiation resistance because the radiation resistance depends on additional parameters of interest such as mass loading and viscoelastic changes and, therefore, is much more sensitive to analyte concentration.

In Figures 4.10-4.21, the change in the radiation resistances is shown for different analyte/coating combinations. The observed radiation resistance is a function of the change in the film's properties: mass loading, viscoelastic changes, change in dielectric constant, and thickness. In addition to the change in radiation resistance, the response time (the time it takes for the response to reach 90% of its steady-state value) can be observed for each of the analyte concentrations. For a given film thickness, there is a given amount of free volume inside the film that the analyte can absorb into. When analyte sorbs into the polymer film, the film swells and changes the thickness. The resistance changes and time responses for each concentration in each experiment is summarized in Tables A.1-A.5 in the Appendix.

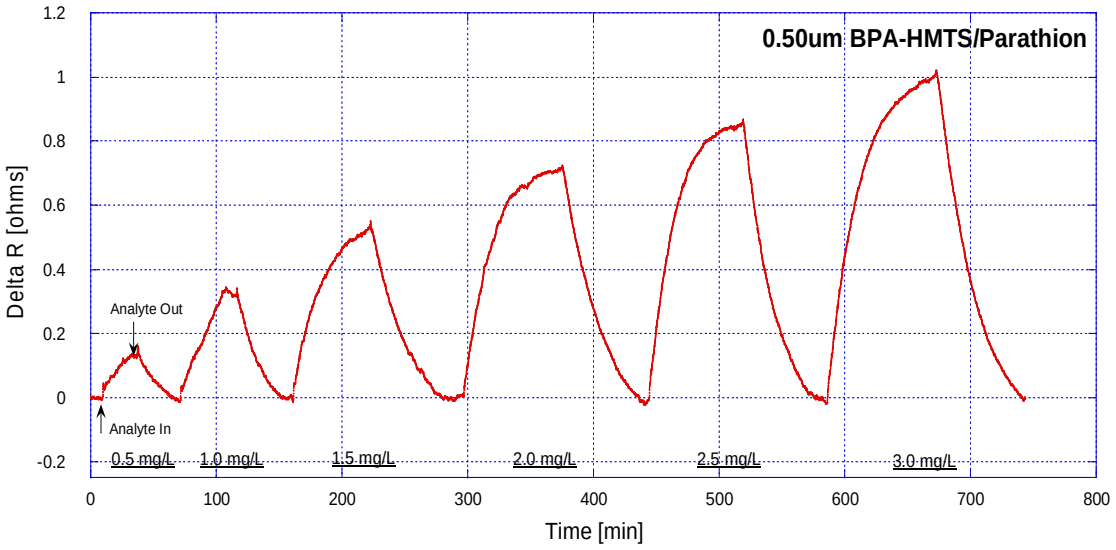

Figure 4.9: Measured change in radiation resistance of the 0.50µm BPA-HMTS coated IDT exposed to 0.5 mg/L, 1.0 mg/L, 1.5 mg/L, 2.0 mg/L, 2.5 mg/L, and 3.0 mg/L of parathion.

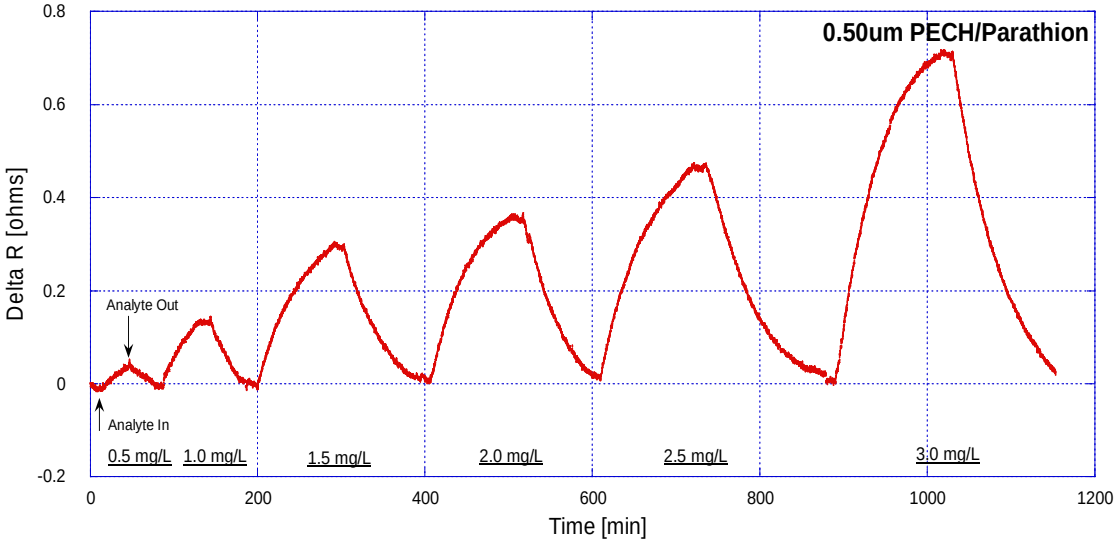

Figure 4.10: Measured change in radiation resistance of the 0.50µm PECH coated IDT exposed to 0.5 mg/L, 1.0 mg/L, 1.5 mg/L, 2.0 mg/L, 2.5 mg/L, and 3.0 mg/L of parathion.

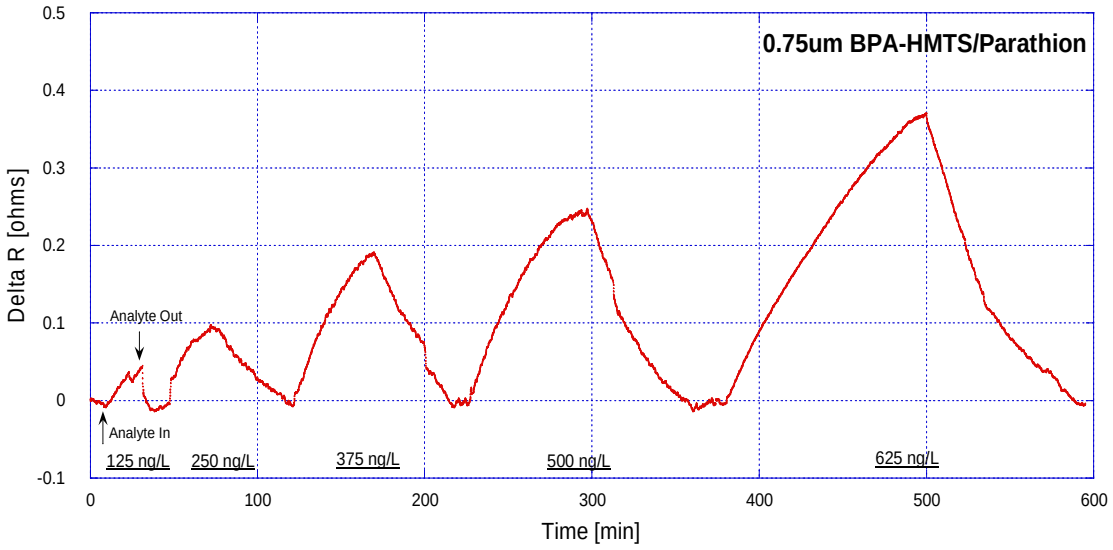

Figure 4.11: Measured change in radiation resistance of the 0.75µm BPA-HMTS coated IDT exposed to 125 ng/L, 250 ng/L, 375 ng/L, 500 ng/L, and 625 ng/L of parathion.

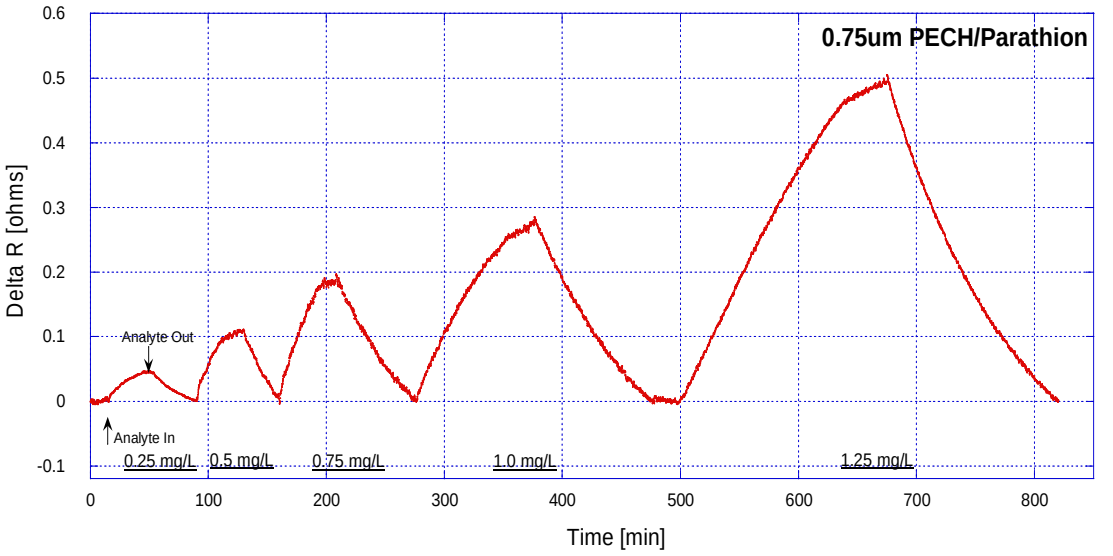

Figure 4.12: Measured change in radiation resistance of the 0.75µm PECH coated IDT exposed to 0.25 mg/L, 0.5 mg/L, 0.75 mg/L, 1.0 mg/L, and 1.25 mg/L of parathion.

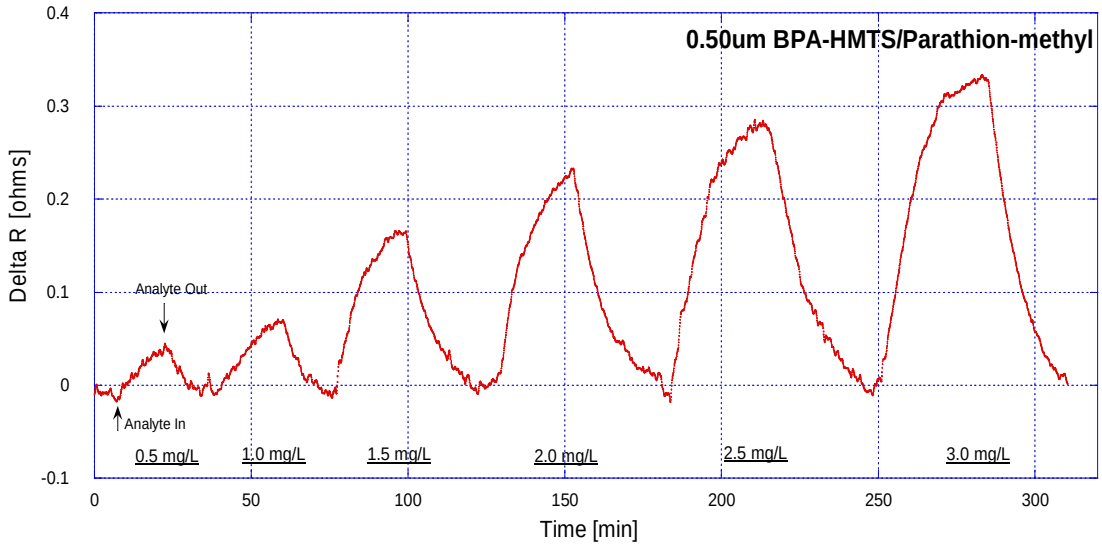

Figure 4.13: Measured change in radiation resistance of the 0.50µm BPA-HMTS coated IDT exposed to 0.5 mg/L, 1.0 mg/L, 1.5 mg/L, 2.0 mg/L, 2.5 mg/L, and 3.0 mg/L of parathion-methyl.

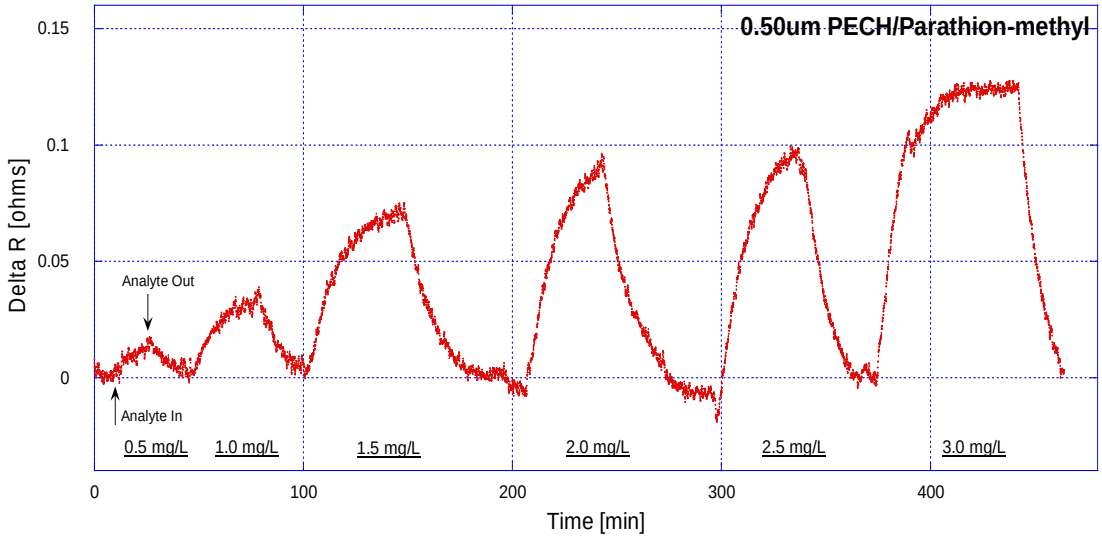

Figure 4.14: Measured change in radiation resistance of the 0.50µm PECH coated IDT exposed to 0.5 mg/L, 1.0 mg/L, 1.5 mg/L, 2.0 mg/L, 2.5 mg/L, and 3.0 mg/L of parathion-methyl.

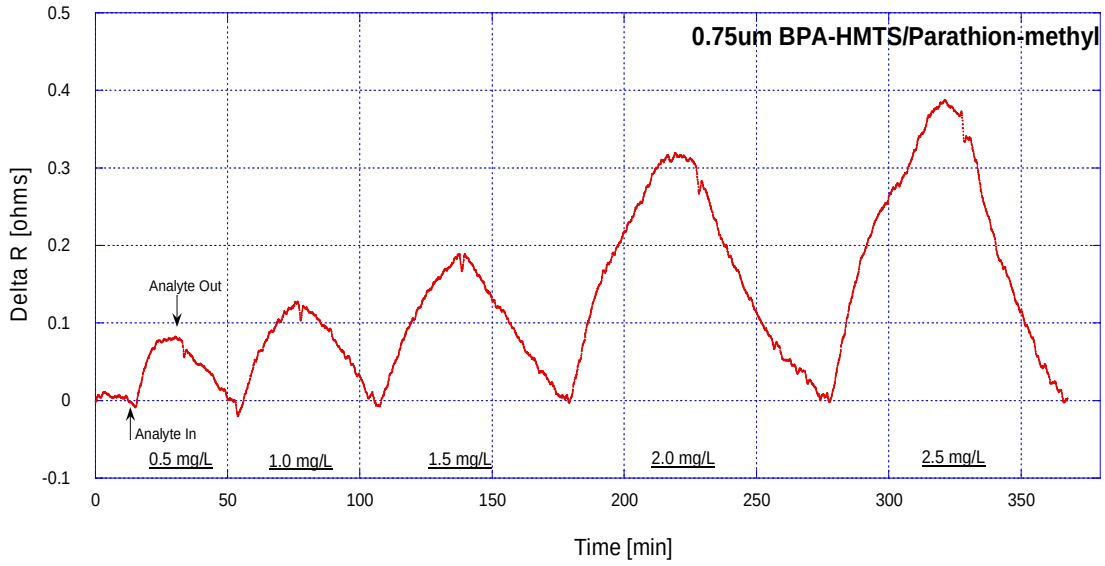

Figure 4.15: Measured change in radiation resistance of the 0.75µm BPA-HMTS coated IDT exposed to 0.5 mg/L, 1.0 mg/L, 1.5 mg/L, 2.0 mg/L, and 2.5 mg/L of parathion-methyl.

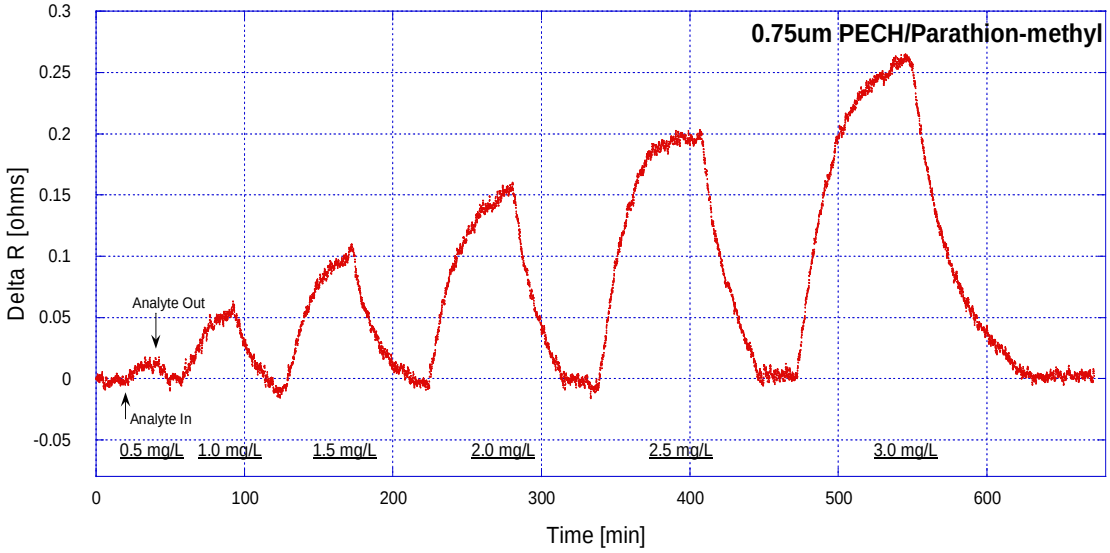

Figure 4.16: Measured change in radiation resistance of the 0.75µm PECH coated IDT exposed to 0.5 mg/L, 1.0 mg/L, 1.5 mg/L, 2.0 mg/L, 2.5 mg/L, and 3.0 mg/L of parathion-methyl.

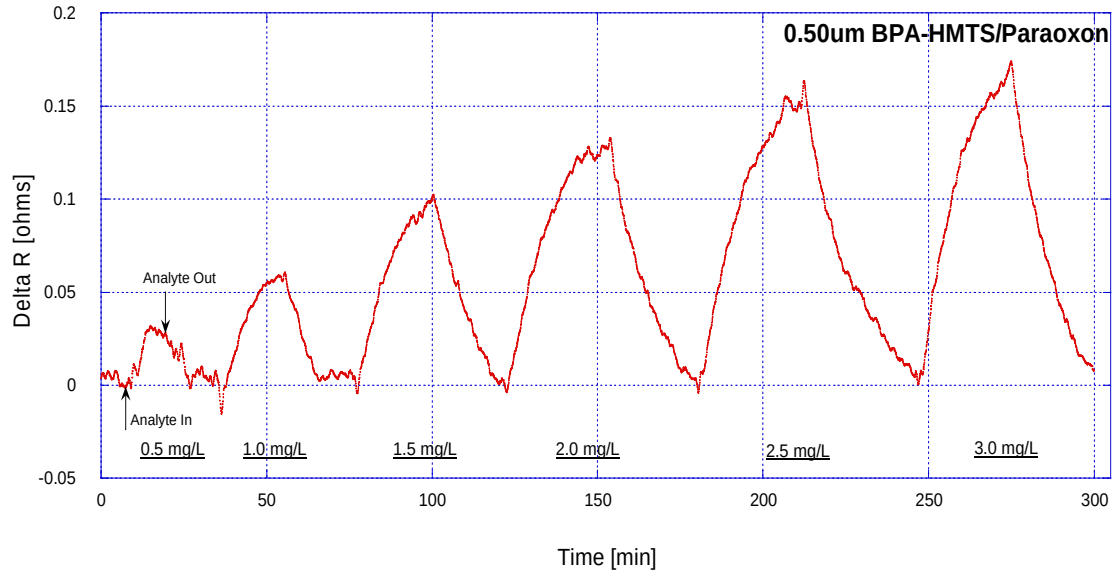

Figure 4.17: Measured change in radiation resistance of the 0.50µm BPA-HMTS coated IDT exposed to 0.5 mg/L, 1.0 mg/L, 1.5 mg/L, 2.0 mg/L, 2.5 mg/L, and 3.0 mg/L of paraoxon.

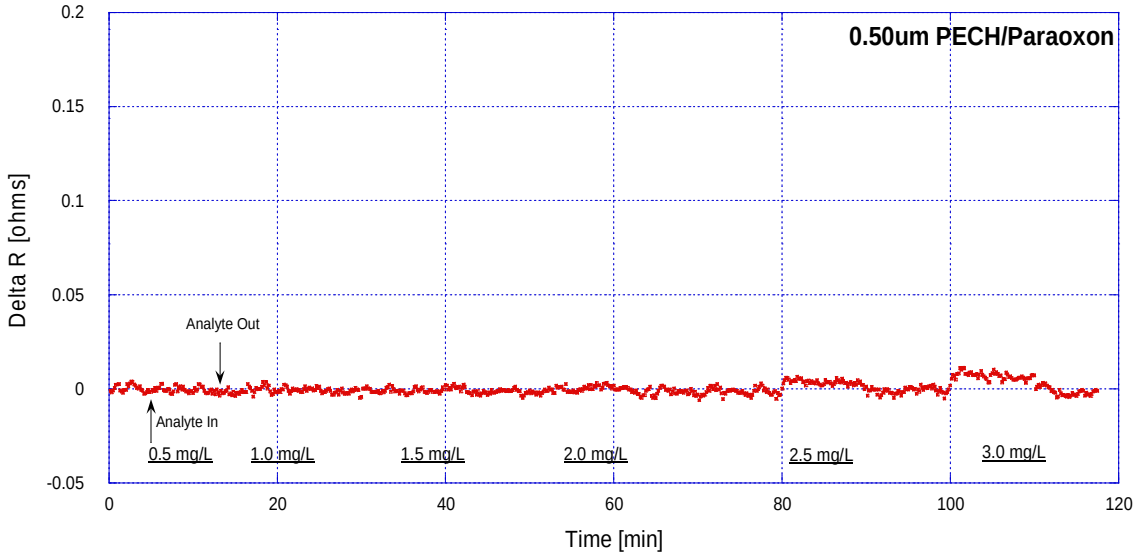

Figure 4.18: Measured change in radiation resistance of the 0.50µm PECH coated IDT exposed to 0.5 mg/L, 1.0 mg/L, 1.5 mg/L, 2.0 mg/L, 2.5 mg/L, and 3.0 mg/L of paraoxon.

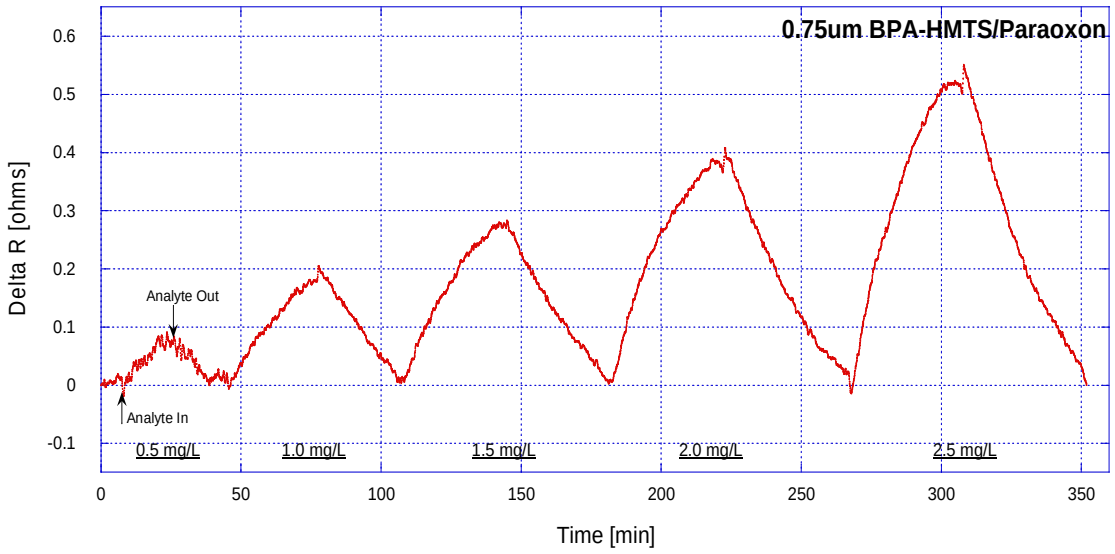

Figure 4.19: Measured change in radiation resistance of the 0.75µm BPA-HMTS coated IDT exposed to 0.5 mg/L, 1.0 mg/L, 1.5 mg/L, 2.0 mg/L, and 2.5 mg/L of paraoxon.

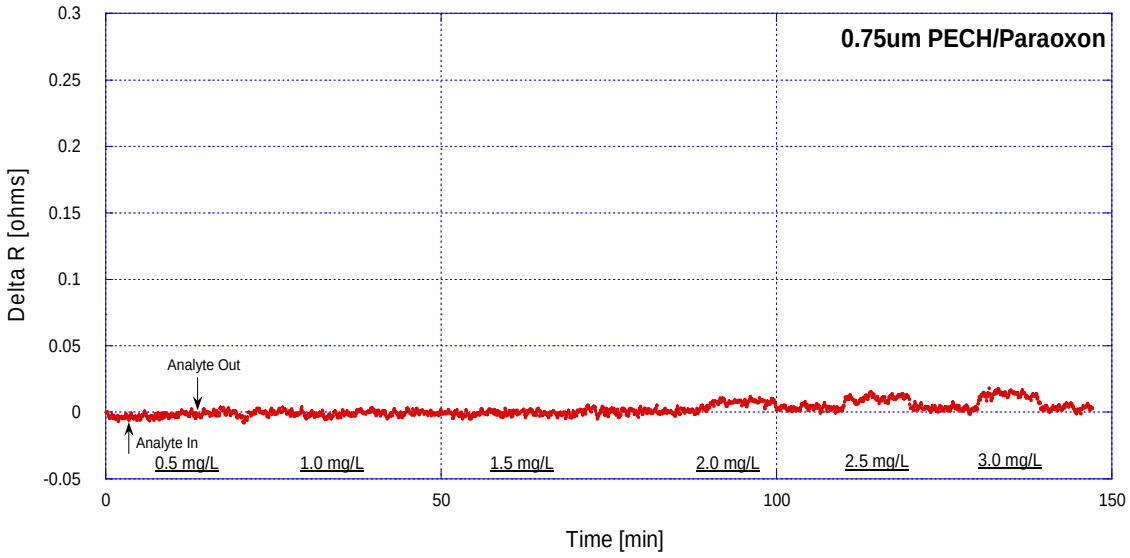

Figure 4.20: Measured change in radiation resistance of the 0.75µm PECH coated IDT exposed to 0.5 mg/L, 1.0 mg/L, 1.5 mg/L, 2.0 mg/L, 2.5 mg/L, and 3.0 mg/L of paraoxon.

The sensitivity of the detection of the three organophosphates varied in terms of coating material and thickness from Figures 4.10-4.21. To more closely compare the overall sensitivities, the sensitivity for each analyte-film combination was calculated using

$$S = \frac{\Delta R}{\Delta C}$$

where ΔR is the change in radiation resistance due to a change in analyte concentration, ΔC. The sensitivity was calculated by plotting the change in the radiation resistance as a function of analyte concentration for a given experiment. A linear fit was then made from the data points where the slope of the line represents the sensitivity. Figures 4.22-4.25 show the sensitivities for each polymer thickness for the sensing of organophosphates. Figures 4.26-4.28 show the sensitivities of the three organophosphates with respect to the different film thicknesses used. The sensitivity data is also summarized in Table A.6-A.7 in the Appendix.

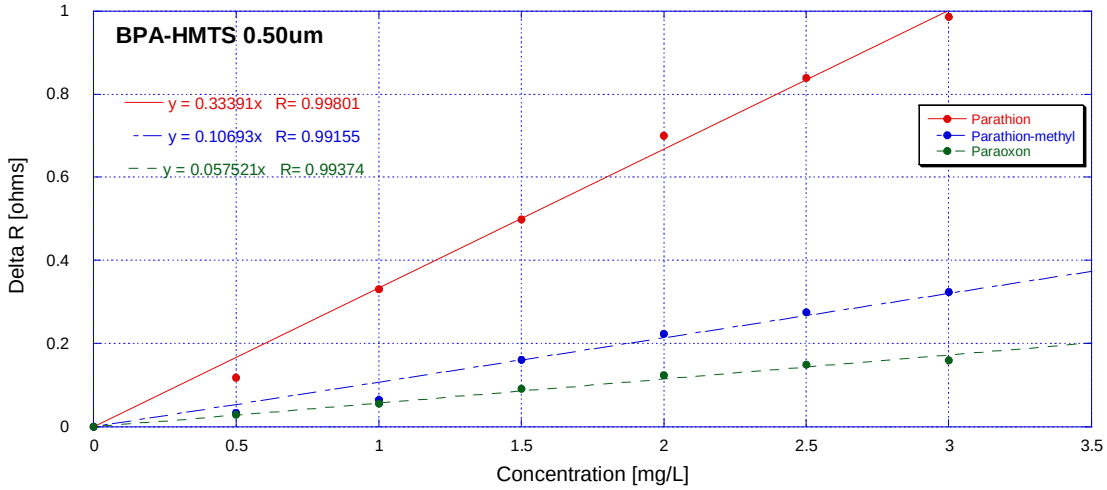

Figure 4.21: Sensitivity curves for the detection of 0.5 mg/L to 3.0 mg/L of parathion, parathion-methyl, and paraoxon using a single IDT guided SH-SAW device coated with 0.50µm of BPA-HMTS.

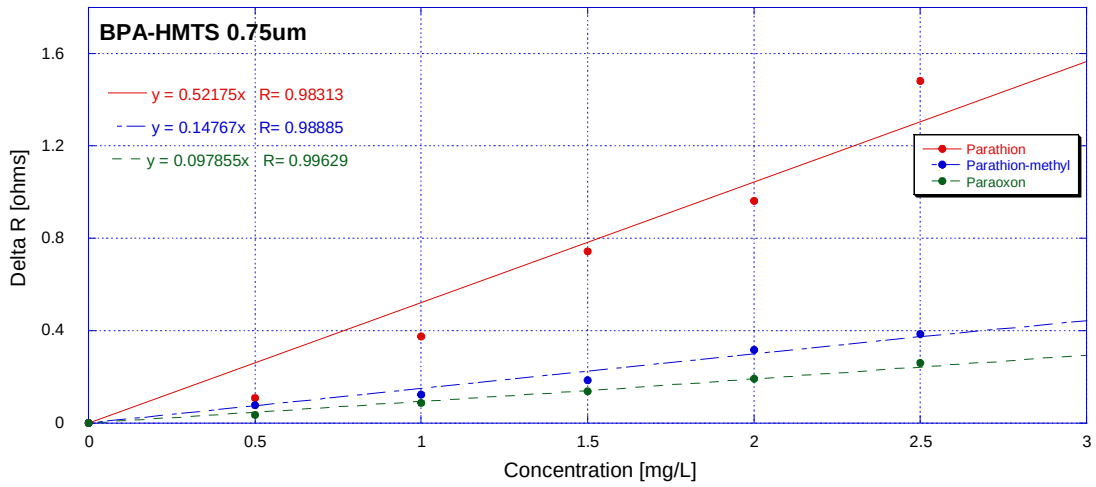

Figure 4.22: Sensitivity curves for the detection of 0.5 mg/L to 3.0 mg/L of parathion, parathion-methyl, and paraoxon using a single IDT guided SH-SAW device coated with 0.75µm of BPA-HMTS.

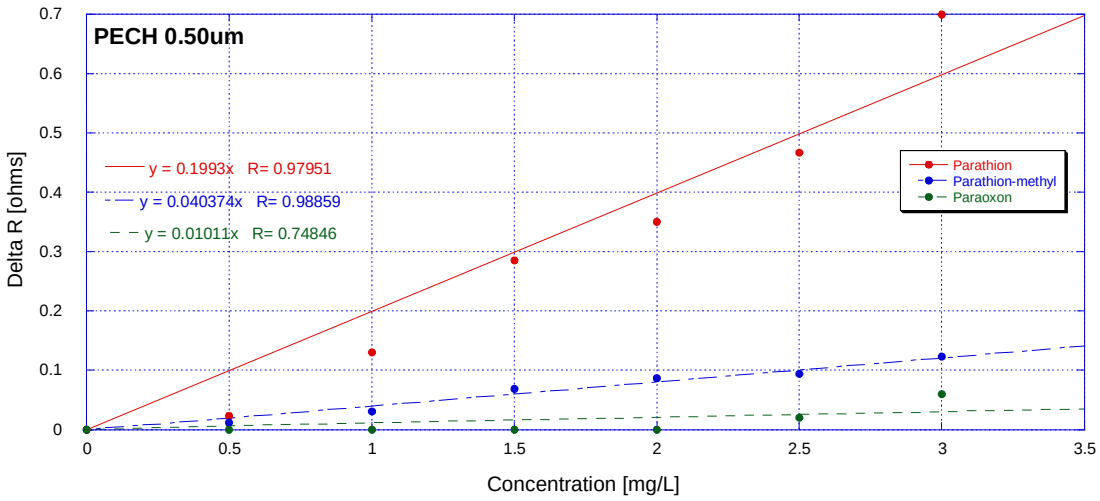

Figure 4.23: Sensitivity curves for the detection of 0.5 mg/L to 3.0 mg/L of parathion, parathion-methyl, and paraoxon using a single IDT guided SH-SAW device coated with 0.50µm of PECH.

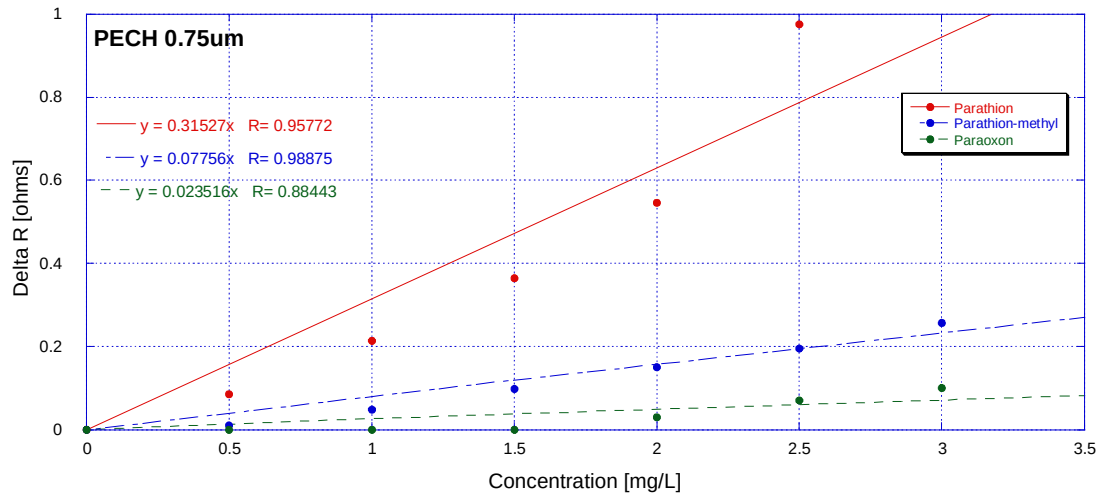

Figure 4.24: Sensitivity curves for the detection of 0.5 mg/L to 3.0 mg/L of parathion, parathion-methyl, and paraoxon using a single IDT guided SH-SAW device coated with 0.75µm of PECH.

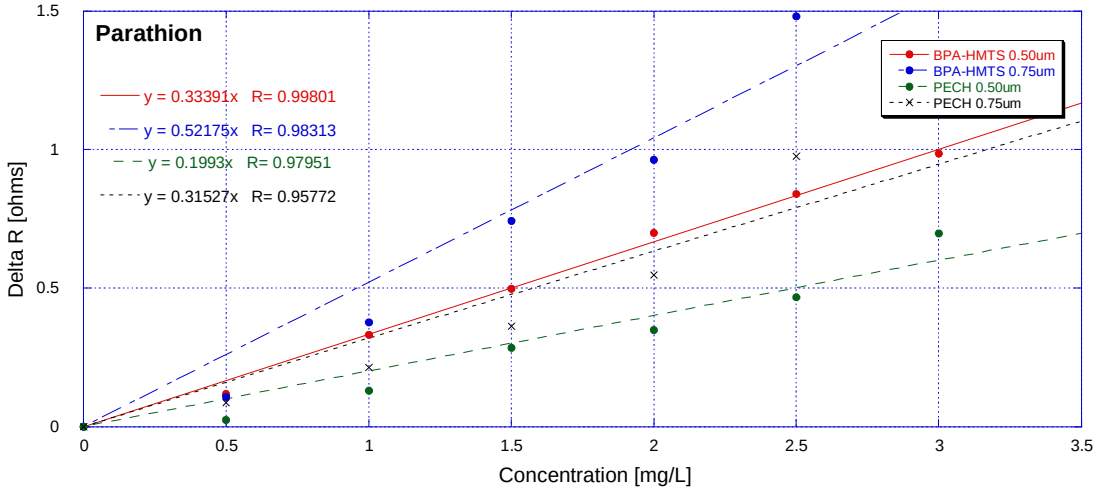

Figure 4.25: Sensitivity curves for the detection of 0.5mg/L to 3.0mg/L of parathion using 0.50µm BPA-HMTS, 0.75µm BPA-HMTS, 0.50µm PECH, and 0.75µm PECH.

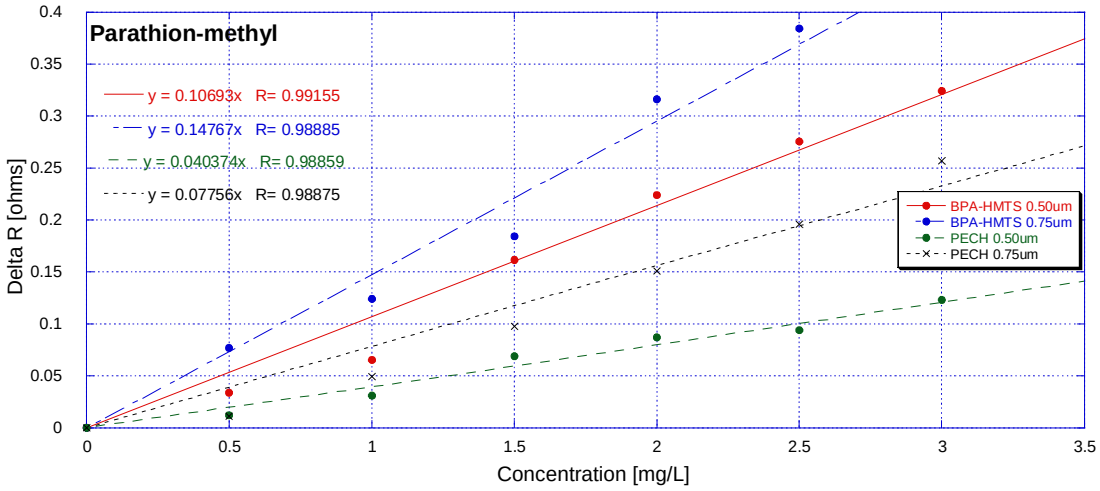

Figure 4.26: Sensitivity curves for the detection of 0.5mg/L to 3.0mg/L of parathion-methyl using 0.50µm BPA-HMTS, 0.75µm BPA-HMTS, 0.50µm PECH, and 0.75µm PECH.

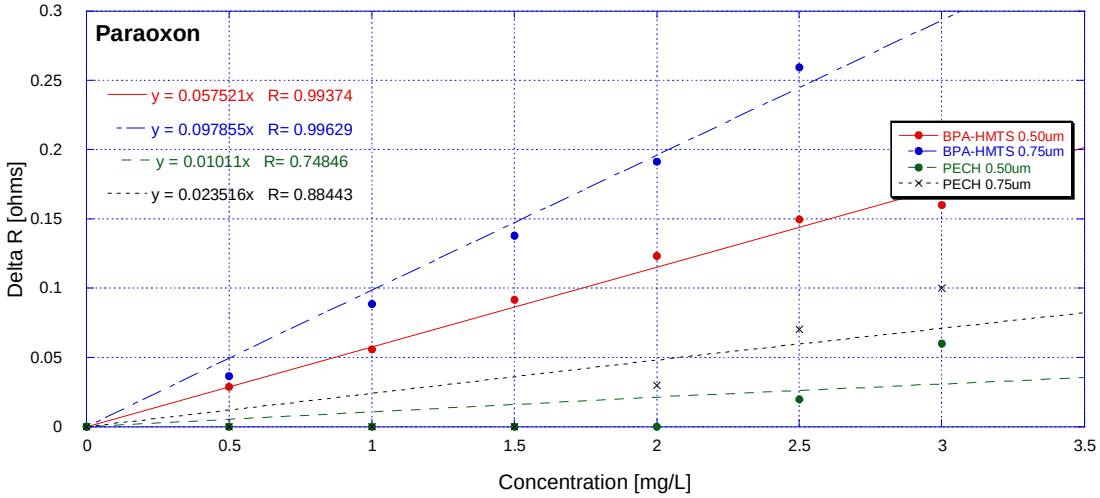

Figure 4.27: Sensitivity curves for the detection of 0.5mg/L to 3.0mg/L of paraoxon using 0.50µm BPA-HMTS, 0.75µm BPA-HMTS, 0.50µm PECH, and 0.75µm PECH.

4.4.2 Discussion of Sensor Responses to Pesticides

Figures 4.10-4.21 show overall that the polymer BPA-HMTS has both greater sensitivity and shorter response times than PECH. Both BPA-HMTS and PECH were most sensitive to least sensitive to parathion, parathion-methyl, and paraoxon respectively from Figures 4.26-4.28. Also, the response time and change in radiation resistance were greater for the 0.75µm thick films than for 0.50µm thick films for both BPA-HMTS and PECH, as expected because of the large sorption volume and longer path for analyte diffusion for the thicker films. Overall, the changes in radiation resistance were mostly linear for increasing concentrations within the investigated concentration ranges. It is also observed that the resistance response is reversible (signal returns back to baseline

after an analyte is removed) which indicates the polymer/analyte interaction is largely physical and that the sensor is reusable.

It can be seen that the response times for parathion can be relatively long, especially for the thicker 0.75μm BPA-HMTS and PECH films. In order to decrease the experiment time, smaller concentration ranges were chosen for these two coatings. This allowed the experiment time to be greatly reduced and demonstrated the capability of the sensors to detect smaller concentrations.

The response time for a polymer/analyte interaction depends on the sensor system (flow rate and cell volume), coating properties, and the sorption kinetics between the analyte and coating. For the given experiments, the flow rate was chosen at 12μL/s and the cell volume is approximately 0.134mL. A higher flow rate can decrease the response time by allowing the cell to be filled/emptied quicker but would introduce noise in the system from turbulence of the liquid flow. A glassier film will exhibit slower response times than a more rubbery film [44]. For physisorption, the porosity of a coating and the dimensions of the analyte molecules will affect the response time [12]. A more porous film subjected to smaller analyte molecules will have shorter response times. Thickness of a film largely contributes to fast or slow response times. A thicker film will have more free volume for the analyte to absorb into, taking more time for the film to be saturated.

The solubility of the organophosphates plays a key role in the overall sensitivity and response time. The solubility of parathion, parathion-methyl, and paraoxon is 12.9mg/L, 38mg/L, and 2400mg/L respectively [33,34,35]. A high solubility means an analyte is more likely to dissolve within the aqueous solution and consequently, less likely to diffuse into the polymer layer. Since all of the organophosphates are similar in

terms of size and density, this explains why paraoxon was shown to have the lowest sensitivity and why parathion had the highest. As a result of having a higher solubility, the response time should be expected to be shorter, since less of the analyte is being absorbed into the coating. Indeed, paraoxon exhibited the quickest response times while parathion had the longest response times.

4.4.3 Sensor Array Design

An important quality for a sensor system is its selectivity. Selectivity is the ability for a chemical sensor system to distinguish one target chemical species from another. Because many times sensors lack perfect selectivity, arrays are often implemented. The sensitivity for a certain chemical will depend on the polymer material. By combining several different chemical sensors into a sensor array, complex chemical mixtures can be analyzed.

A sensor array can be designed by either combining sensor information from discretely-tested devices or by combining several devices onto one chip. At the current stage of development, the sensor array will be designed from data collected from discrete coated devices. Because many polymers are partially-selective, more than one is required to create a sensor array. For this work, BPA-HMTS and PECH will be the two polymer choices for the array. The measurements from the two polymers that will be used as the input parameters are chosen so that the two are independent of each other. For this work, the change in the radiation resistance and response time were measured. This gives a total of four input parameters, two from each polymer, to develop analyte-specific patterns. These patterns can then be recognized using pattern recognition techniques.

The frequency shift associated with the detection of the same organophosphates using the same two polymers using a delay-line SH-SAW device has been investigated by Newman [37]. This data will also be implemented into the sensor array. As mentioned, the input parameters cannot be independent of each other, this means that only one thickness may be used. The thickness in common with this work and from Newman that will be used for the sensor array is 0.5μm. The six input parameters for the sensor array are summarized in Table 4.1.

BPA-HMTS	PECH
Resistance change [Ω]	Resistance change [Ω]
Response time [min]	Response time [min]
Frequency shift [kHz]	Frequency shift [kHz]

Table 4.1: Sensor array design using BPA-HMTS and PECH coated devices at a thickness of 0.5μm.

Figures 4.29-4.31 show a visual pattern recognition technique using radial plots for parathion, parathion-methyl, and paraoxon at concentrations from 0.5mg/L to 3.0mg/L. The axes of the radial plots are the six input parameters: resistance change, response time, and frequency shift for both BPA-HMTS and PECH. The values for the radial plots can be found in Tables A.1-A.5 in the Appendix. The frequency shift, time response, and resistance change are all normalized to the largest response for comparison.

From the radial plots in Figure 4.29 (a-f), Figure 4.30 (a-f), and Figure 4.31(a-f) it can be seen that each organophosphate has a unique visual pattern. These patterns are also fairly consistent throughout all concentrations. Single-analyte detection is more accurately obtained now by use of the recognition patterns. One can take an unknown

sample, assuming to be one of the three organophosphates from 0.5mg/L to 3.0mg/L, and be able to correctly identify the analyte and concentration from measuring the input parameters.

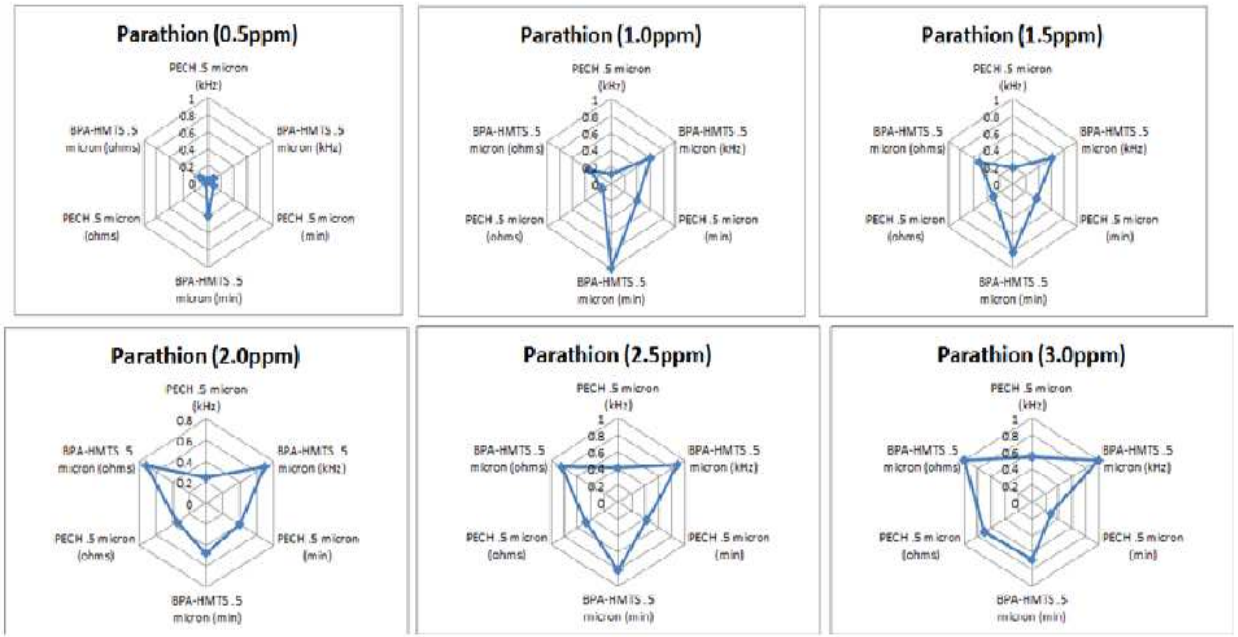

Figure 4.28: Radial plots showing the detection of parathion at concentrations of (a) 0.5mg/L , (b) 1.0mg/L, (c) 1.5mg/L , (d) 2.0mg/L, (e) 2.5mg/L, and (f) 3.0mg/L using BPA-HMTS and PECH at thickness 0.5µm in an array. The resistance change, frequency shift, and time response are normalized.

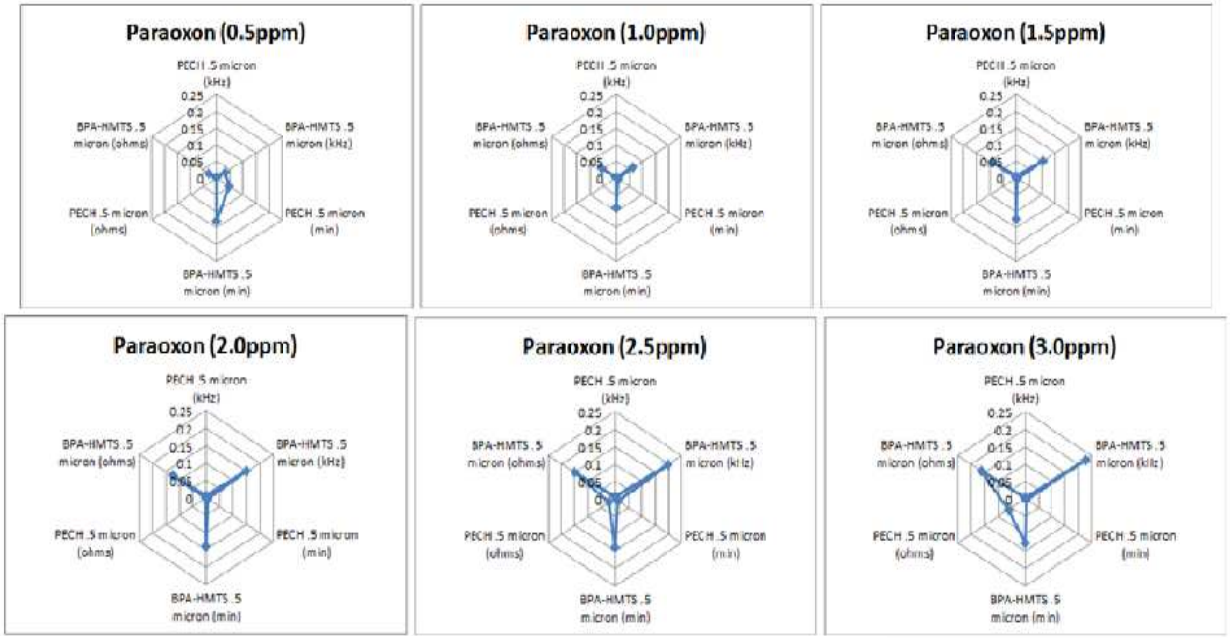

Figure 4.29: Radial plots showing the detection of paraoxon at concentrations of (a) 0.5mg/L , (b) 1.0mg/L, (c) 1.5mg/L , (d) 2.0mg/L, (e) 2.5mg/L, and (f) 3.0mg/L using BPA-HMTS and PECH at thickness 0.5µm in an array. The resistance change, frequency shift, and time response are normalized.

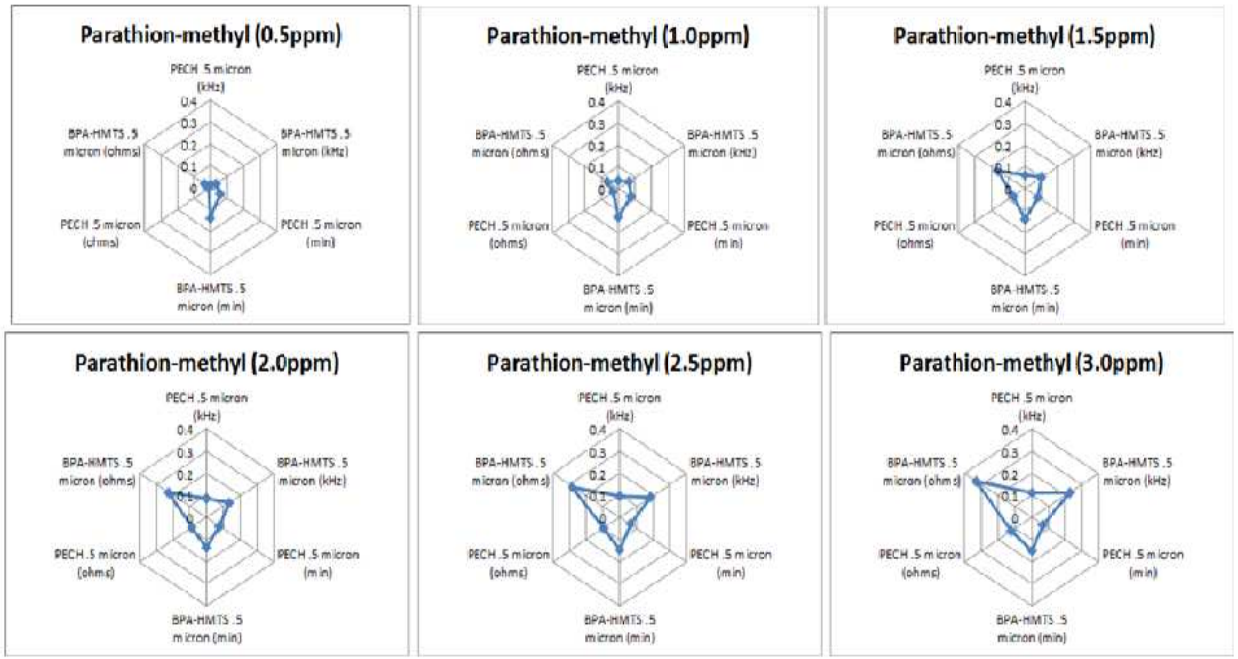

Figure 4.30: Radial plots showing the detection of parathion-methyl at concentrations of (a) 0.5mg/L , (b) 1.0mg/L, (c) 1.5mg/L , (d) 2.0mg/L, (e) 2.5mg/L, and (f) 3.0mg/L using BPA-HMTS and PECH at thickness 0.5µm in an array. The resistance change, frequency shift, and time response are normalized.

4.4.4 Polymer Reproducibility

The synthesis of BPA-HMTS is rather complex and is performed at Marquette University whereas PECH is readily available in solid form and only needs to be dissolved. After BPA-HMTS is synthesized and stored, slight variations in the film occur over time that affect its sensing capabilities. Physically, the film becomes harder and its color turns into a dark brown. An experiment was performed to test two samples of BPA-HMTS that were synthesized at different times. One sample was synthesized and has been stored for over a year before testing and another was made just a week before testing. Figure 4.32 shows the comparison between the two samples of BPA-HMTS for the detection of parathion from 0.5mg/L to 3.0mg/L. The newer synthesized BPA-HMTS has a slightly greater response and shorter response time than the older synthesized BPA-HMTS. Most noticeable is the difference in linearity between the two samples. The responses for the newer BPA-HMTS are much more linear with concentration than those of the older BPA-HMTS, this is more easily seen in Figure 4.33. These results highlight the necessity to find methods of synthesis and storage that will ensure a reproducible performance of the BPA-HMTS coatings.

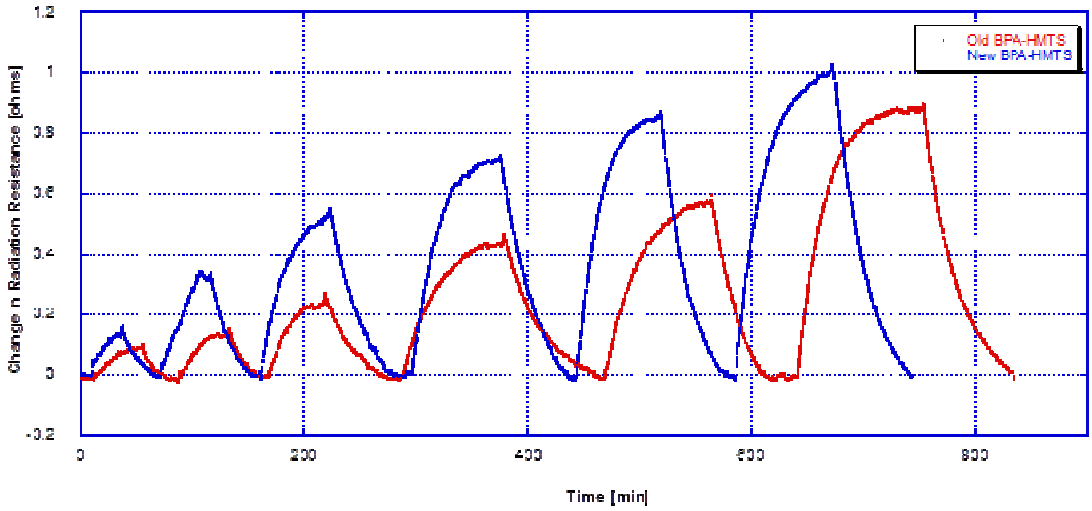

Figure 4.32: Comparison of old and new BPA-HMTS for the detection of parathion from 0.5mg/L to 3.0mg/L

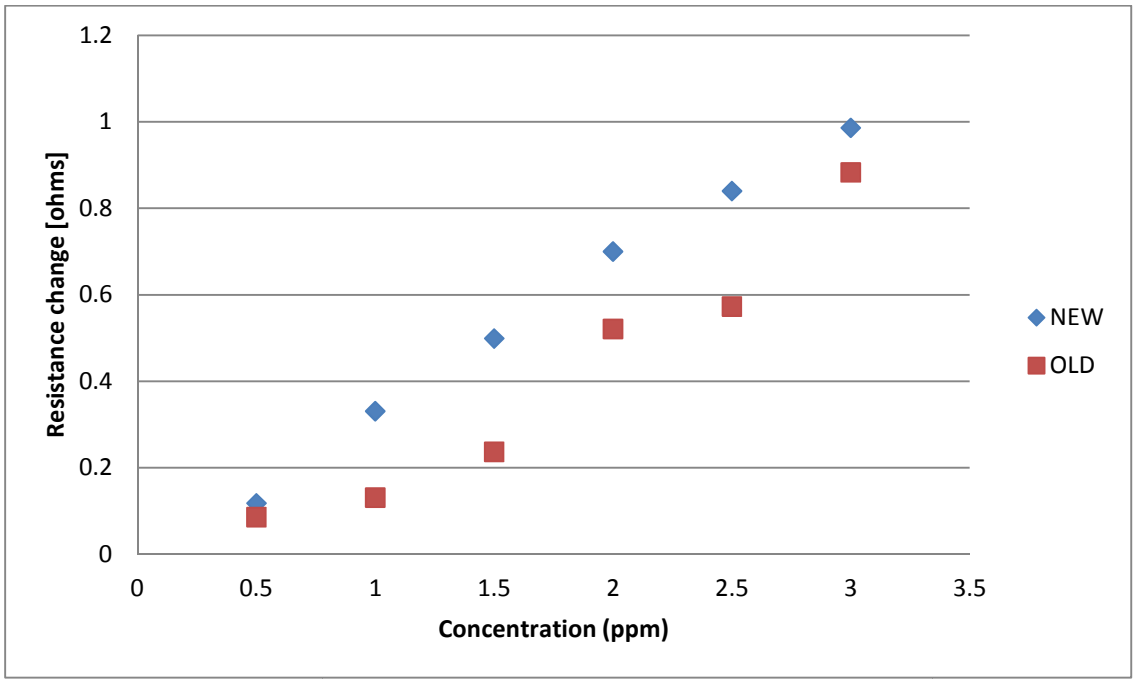

Figure 4.32: Comparison of old and new BPA-HMTS for the detection of parathion from 0.5mg/L to 3.0mg/L

5. SUMMARY, CONCLUSIONS, AND FUTURE WORK

5.1 Summary

The objective of this work was to investigate the usability of a coated single IDT sensor for the direct detection of organophosphates in aqueous solutions. Two partially-selective films were selected and evaluated in terms of their sensitivity and selectivity to the organophosphates. Selectivity was enhanced by use of visual pattern recognition techniques by combining several measurable quantities in an array. The influence of aging of polymer coatings on the reproducibility of their performance in sensor measurements was discussed.

A background on organophosphate pesticides was discussed along with a rationale for developing sensors capable of rapid, in-situ detection of organophosphate pesticides. An overview of chemical sensors was then discussed with an emphasis on acoustic wave based chemical sensors utilizing the interdigital transducer. The interdigital transducer was then introduced with a brief description.

The theory of the interdigital transducer was carefully discussed in Chapter 2. The geometry was first presented along with the principle of operation via the piezoelectric effect. An equivalent circuit model was given to simplify the analysis and theory of the IDT. The circuit elements were carefully derived. Changes in the circuit model were then evaluated for the dielectric film loaded case and aqueous solution case. A final circuit model encompassing all the changes to the sensor for the case of liquid-phase sensing was presented.

Detailed procedures for the synthesis and/or preparation of BPA-HMTS and PECH polymers and organophosphate samples were outlined in Chapter 3. Brief descriptions of the instruments used in these procedures were given. The experimental setup was depicted in Figure 3.x along with a description as to how the data is collected and processed.

Two partially-selective polymers (BPA-HMTS and PECH) were used and tested for the detection of three organophosphates (parathion, parathion-methyl, and paraoxon) in Chapter 4. The concentrations tested for the organophosphates ranged from 125ppb to 3.0ppm. Two thicknesses (0.50μm and 0.75μm) were tested for each polymer. The change in the radiation resistance and the response time were extracted from the measured response. A linear fit was made to calculate the sensitivity for each polymer/analyte case. The two polymers were evaluated in terms of their sensitivity to each of the three organophosphates. Selectivity was enhanced by forming a sensor array with multiple input parameters to develop specific analyte patterns. Finally, the reproducibility in the performance of BPA-HMTS was discussed with respect to the polymer solution aging.

5.2 Conclusions

In this work, it was shown that a single IDT coated with a selective polymer can be used for sensing in liquid phase. Specifically, this work showed that single IDTs coated with the polymers BPA-HMTS and PECH can be used for the detection of organophosphates in an aqueous solution. The sensor response, the change in radiation resistance, was shown to be a linear function of the mass loading, viscoelastic changes,

dielectric changes, and changes in film thickness. The 0.75μm thick films showed greater responses than the 0.50μm films due to increased free volume for the analytes to absorb into. BPA-HMTS had both greater sensitivity and shorter response times than PECH. This was due to BPA-HMTS having more free volume, allowing more sorption of analyte and faster analyte diffusion through pores [44]. Both films were most sensitive to least sensitive to parathion, parathion-methyl, and paraoxon respectively. This is explained from the solubility of the three organophosphates. Paraoxon has the highest solubility in water and so less of the analyte is going to absorb into the film, rather it will dissolve in the aqueous solution instead. Because of this, paraoxon showed the lowest sensitivity out of the three organophosphates for both BPA-HMTS and PECH. Parathion on the other hand has a much lower solubility than the other analytes and so showed the greatest responses. Other factors that affect sensor response time are the dimensions of the analyte and porous coating.

In order to increase sensor selectivity, a sensor array was used to create distinguishable patterns for each organophosphate. These patterns can then be recognized using various pattern recognition techniques. It is shown that each organophosphate has, within certain error margins, a distinct pattern that can be used to distinguish one from the others. The axes from the radial plots are the change in radiation resistance, sensor response time, and frequency shift (from Newman [x]) for both BPA-HMTS and PECH. The patterns of the three organophosphates remained relatively similar for varying concentrations with the magnitudes of the axes increasing for higher concentrations.

The polymer BPA-HMTS was tested for reproducibility after it had been aged for over a year. The test consisted of testing two different samples of BPA-HMTS, one a year old and the other less than a week old. The results, under the same conditions, showed that the aged BPA-HMTS exhibited less sensitivity and longer response times than the newly synthesized BPA-HMTS sample. This may be related to the fact that physically the aged BPA-HMTS hardened over time and was more difficult to dilute in chloroform than the newly-made sample. The film itself was probably harder which reduced analyte absorption into the polymer, leading to a reduced response.

5.3 Future Work

This work offers many opportunities for future improvements. Desirable improvements include producing more reliable polymers and designing a more efficient and accurate sensor array. The polymer BPA-HMTS, which is synthesized here at Marquette University, is very difficult to reproduce identically. This leads to slight variations in polymer coating properties when performing experiments. More investigation can be done to simplify the synthesis procedures to create a more reliable polymer. Ways of improving the shelf life of BPA-HMTS needs to be looked at also. From Figure 4.32, the sensor response for BPA-HMTS gradually decreases for extended time periods. This may be circumvented if there were storage techniques to preserve the polymer longer.

The sensor array can be improved. This work used only two polymer coatings for the selectivity of organophosphates. Different polymers should be investigated that are partially-selective to organophosphates and used for the sensor array. More

concentrations could be measured rather than from 0.125mg/L to 3.0mg/L, to further explore the detection limits for various coating/analyte combinations. The accuracy of the sensor array would be improved if all the devices were combined onto one wafer, as opposed to measuring each device separately. Data collection can become much more efficient because all the devices are being tested at one time. Also, the accuracy of the experiments would be improved because every device is subjected to the same testing conditions. A process to individually coat multiple IDTs on a single device can be proposed.

In addition, the film thicknesses chosen to detect organophosphates need to be investigated further. For this work, only 0.50μm and 0.75μm thick films were used. For the purpose of an array, two non-similar thicknesses needed to be used. It is possible that for each polymer, an ideal thickness exists that is most sensitive to organophosphates. Thicker films, beyond 0.75μm, may be able to show larger responses to organophosphates, due to increased free space volume, without damping the acoustic wave. This can lead to the detection of smaller concentrations. However, the choice for the optimum coating thickness should also take into account the response time observed for each coating/analyte combination.

REFERENCES

1. “Organophosphate Insecticides”, [Online]. Available: http://npic.orst.edu/RMPP/rmpp_ch4.pdf [Accessed 14 July 2013].

2. Katz D.K, ‘Organophosphate Toxicity’, Medscape, [Online]. Available: http://emedicine.medscape.com/article/167726-overview [Accessed 15 July 2013].

3. “Nerve Agent and Organophosphate Pesticide Poisoning”, Centers for Disease Control and Prevention, 14 Feb 2013.

4. Lee, P., Tai, D., ‘Clinical features of patients with acute organophosphate poisoning requiring intensive care’, *Intensive Care Medicine*, Vol. 27, no. 4, pp. 694-699.

5. “Pesticides in Groundwater”, [Online]. Availabe: http://ga.water.usgs.gov/edu/pesticidesgw.html [Accessed 14 July 2013].

6. Tankiewicz, M., Fenik, J., Biziuk, M., ‘Determination of organophosphorus and organonitrogen pesticides in water samples’, *Analytical Chemistry*, Vol. 29, no. 9, pp. 1050-1063.

7. J. R. Stetter, W. R. Penrose and S. Yao, "Sensors, Chemical Sensors, Electrochemical Sensors, and ECS," *Journal of The Electrochemical Society,* vol. 150, no. 2, pp. S11-S16, 2003.

8. “An Introduction to Sensors and Transducers”, [Online]. Available: http://www.mfg.mtu.edu/cyberman/machtool/machtool/sensors/intro.html [Accessed 15 July 2013].

9. Hulanicki, A., Glab, S., and Ingman, F., ‘Chemical sensors definitions and classifications’, Pure & Appl. Chem., Vol. 63, No. 9, pp. 1247-1250, 1991.

10. Pallás-Areny, Ramón, and John G. Webster. *Sensors and Signal Conditioning*. New York: Wiley, 2001.

11. B. Drafts, "Acoustic Wave Technology Sensors," *IEEE Transactions on Microwave Theory and Techniques,* vol. 49, no. 4, pp. 795-802, 2001.

12. D. S. Ballantine, R. M. White, S. J. Martin, H. Wohltjen and A. J. Ricco, Acoustic Wave Sensors: Theory, Design, and Physico-Chemical Applications, San Diego: Academic Press, 1997.

13. Herrmann, F., Weihnacht, M., Buttgenbach, S., ‘Properties of sensors based on shear-horizontal surface acoustic waves in LiTaO3/SiO2 and quartz/SiO2 structures’, IEEE Trans. UFFC, vol. 48, no. 1, pp. 268-273, 2001.

14. S. J. Martin, G. C. Frye and S. D. Senturia, "Dynamics and Response of Polymer-Coated Surface Acoustic Wave Devices: Effect of Viscoelastic Properties and Film Response," *Anal. Chem.*, vol. 66, pp. 2201-2219, 1994.

15. Morgan, D.P.: 'Surface acoustic wave devices and applications – 1. Introductory review', Ultrasonics, 1973, 11, pp. 121-131.

16. Engan, H.: 'Excitation of elastic surface waves by spatial harmonics of interdigital transducers', IEEE Trans., 1969, ED-16, pp. 1014-1017.

17. F. Josse, F. Bender and R. W. Cernosek, "Guided shear horizontal surface acoustic wave sensors for chemical and biochemical detection in liquids," *Anal. Chem.*, vol. 73, pp. 5937-5944, 2001.

18. A. K. Mensah-Brown, "Detection of Organophosphates in the Liquid-Phase Using Guided SH-SAW Sensors [Thesis]," Marquette University, Milwaukee, 2007.

19. White, R.M., and Voltmer, F.W.: 'Direct piezoelectric coupling to surface elastic waves', Appl Phys. Lett., 1965, 7, pp. 314-316.

20. Milsom, R.F., Redwood, M., 'Piezoelectric generation of surface waves by interdigital array', Proc. IEE, 1971, 118, pp.831-840.

21. Coquin, G.A., and Tiersten, H.F.: 'Analysis of the excitation and detection of piezoelectric surface waves in quartz by means of surface electrodes', J. Acoust. Soc. Amer., 1967, 41, pp.921-939.

22. Redwood, M., and Milsom, R.F.: 'Piezoelectric coupling coefficient of interdigital Rayleigh-wave transducer', Electron. Lett., 1970, 6, p.437.

23. B.A. Auld, Acoustic Fields and Waves in Solids, Vol. 1, A Wiley-Interscience Pubication, New York, (1973)

24. Solie, L.P., 'Piezoelectric waves on layered substrates', Hansen Laboratories of Physics, Stanford University, Stanford, California.

25. Smith, W.R., Gerard, H.M., Collins, J.H., Reeder, T.M., and Shaw, H.J.: 'Analysis of interdigital surface wave transducers by use of an equivalent circuit model', IEEE Trans., 1969, MTT-17, pp. 856-864

26. Gevorgian, S., Berg, H.: 'Line capacitance and impedance of coplanar strip waveguides on substrates with multiple dielectric layers', Chalmers University of Technology, Gothenburg, Sweden.

27. Abu-Abed, A.S., Lindquist, R.G., 'Capacitive interdigital sensor with inhomogeneous nematic liquid crystal film', Progress in Electromagnetics Research B, Vol. 7, pp. 75-87, 2008.

28. Kovacs, G., Lubking, G.W., Vellekoop, M.J., and Venema, A.: 'Love waves for (bio)chemical sensing in liquids', IEEE Ultrasonics Symposium, 1992, pp. 281-285.

29. R. Sethupathi, "A Single-IDT Acoustic Wave Sensor for Viscoelastic Dielectric Film Media [Thesis]", Marquette University, Milwaukee 1992.

30. Stone, D.C., Thompson, M.: 'Interdigital capacitance and surface acoustic wave sensors', Anal. Chem., vol. 65, 1993, p352.

31. "Lithium Niobate/Lithium Tantalae acoustic crystals", Crystal Technology Inc., Palo Alto, California.

32. F. Josse, Marquette University.

33. "Parathion". Geneva, World Health Organizations, Internation Programme on Chemical Safety (Environmental Health Criteria 145).

34. "Methyl parathion". Geneva, World Health Organizations, Internation Programme on Chemical Safety (Environmental Health Criteria 145).

35. Pickering, W.R., 'Paraoxon', Biochem. Pharmacol., 16, 1183 (1967).

36. A. K. Mensah-Brown, "Analysis of the Detection of Organophosphate Pesticides in Aqueous Solutions Using Polymer-Coated SH-SAW Devices [Dissertation]," Marquette University, Milwaukee, 2010.

37. T. Newman, "Analysis of the Detection of Organophosphate Pesticides in Aqueous Solutions Using Polymer-Coated SH-SAW Sensor Arrays [Thesis]," Marquette University, Milwaukee 2012.

38. "Spin Coating Theory", 2012. [Online]. Available: http://www.cise.columbia.edu/clean/process/spintheory.pdf. [Accessed 19 June 2013]

39. Quartz reference

40. "Ellipsometers," Gaertner Scientific Corporation , 2008-2012. [Online]. Available: http://www.gaertnerscientific.com/ellipsometers/main.htm. [Accessed 19 June 2013].

41. F. Josse and R. Cernosek.

42. Natale, C.D., Davide A.M., and D'Amico, A., 'A self-organizing system for pattern classification: time-varying statistics and sensor drift effects', Sensors and

Actuators, B26-27, 1995, pp. 237-241.

43. Datasheet of Lithium Tantalate device

44. Grate, J., Nelson, D., ‘Sorptive polymeric materials and photopatterned films for gas phase chemical microsensors’, Proc. IEEE, Vol. 91, No. 6, 2003, p.881-889.

APPENDIX

Figure A.1: Geometry of split-finger transducer

$$C_T = N\varepsilon_{eff}W \cdot \left[0.55 + 0.85 \cdot e^{1.75(\alpha - 0.5)}\right] \quad \text{(A.1)}$$

	Resistance Change (Ω)		Time Response (min)	
Film / Analyte	PECH (0.5µm)	BPA-HMTS (0.5µm)	PECH (0.5µm)	BPA-HMTS (0.5µm)
Parathion (0.5mg/L)	0.024	0.118	30	25.2
Parathion (1.0mg/L)	0.13	0.331	49.2	43.5
Parathion (1.5mg/L)	0.285	0.499	94.8	58.2
Parathion (2.0mg/L)	0.35	0.7	105.6	72.9
Parathion (2.5mg/L)	0.467	0.84	124.2	70.5
Parathion (3.0mg/L)	0.699	0.986	132.6	84.3

Table A.1: The resistance change and response time for 0.5µm thick BPA-HMTS and PECH films exposed to parathion concentrations from 0.5mg/L to 3.0mg/L

	Resistance Change (Ω)	Time Response (min)
Film / Analyte	PECH (0.75µm)	PECH (0.75µm)
Parathion (0.25mg/L)	0.043	33.5
Parathion (0.50mg/L)	0.107	40.5
Parathion (0.75mg/L)	0.182	43.3
Parathion (1.00mg/L)	0.273	95.1
Parathion (1.25mg/L)	0.488	163.5

Table A.2: Resistance change and response time for 0.75µm thick PECH film exposed to parathion concentrations from 0.25mg/L to 1.25mg/L

	Resistance Change (Ω)	Time Response (min)
Film / Analyte	BPA-HMTS (0.75µm)	BPA-HMTS (0.75µm)
Parathion (0.125mg/L)	0.027	18.3
Parathion (0.250mg/L)	0.094	24.2
Parathion (0.375mg/L)	0.186	46.4
Parathion (0.500mg/L)	0.241	68.3
Parathion (0.625mg/L)	0.37	120.5

Table A.3: Resistance change and response time for 0.75µm thick BPA-HMTS film exposed to parathion concentrations from 0.125mg/L to 0.625mg/L.

	Resistance Change (Ω)				Time Response (min)			
Film / Analyte	PECH 0.5µm	BPA-HMTS 0.5µm	PECH 0.75µm	BPA-HMTS 0.75µm	PECH 0.5µm	BPA-HMTS 0.5µm	PECH 0.75µm	BPA-HMTS 0.75µm
PM (0.5mg/L)	0.012	0.0337	0.011	0.077	13.7	14.2	19.4	12.5
PM (1.0mg/L)	0.031	0.0654	0.049	0.124	28	17.9	34.3	22
PM (1.5mg/L)	0.069	0.1615	0.098	0.184	43.9	19.6	40.2	31.3
PM (2.0mg/L)	0.087	0.2238	0.151	0.316	37.8	23.8	53.9	42.2
PM (2.5mg/L)	0.094	0.2757	0.196	0.384	37.2	28.8	61.8	46.9
PM (3.0mg/L)	0.123	0.3238	0.257	-	48.6	30.9	74.4	-

Table A.4: Resistance change and response time for 0.50µm and 0.75µm thick PECH and BPA-HMTS films exposed to parathion-methyl concentrations from 0.5mg/L to 3.0mg/L.

	Resistance Change (Ω)				Time Response (min)			
Film / Analyte	PECH 0.5µm	BPA-HMTS 0.5µm	PECH 0.75µm	BPA-HMTS 0.75µm	PECH 0.5µ	BPA-HMTS 0.5µm	PECH 0.75µm	BPA-HMTS 0.75µm
Paraoxon (0.5mg/L)	n/a	0.0288	n/a	0.073	n/a	9.9	n/a	18.2
Paraoxon (1.0mg/L)	n/a	0.0558	n/a	0.177	n/a	15.9	n/a	30.7
Paraoxon (1.5mg/L)	n/a	0.0916	n/a	0.276	n/a	22.3	n/a	34.8
Paraoxon (2.0mg/L)	n/a	0.1235	0.03	0.383	0	29	4	37.7
Paraoxon (2.5mg/L)	0.02	0.1496	0.07	0.519	4.1	30.9	5.5	36
Paraoxon (3.0mg/L)	0.06	0.16	0.01	-	4.5	27	8.5	-

Table A.5: Resistance change and response time for 0.50µm and 0.75µm thick PECH and BPA-HMTS films exposed to paraoxon concentrations from 0.5mg/L to 3.0mg/L.

Sensitivity ΔR (ohms/ppm)			
Analyte	Film Thickness	PECH	BPA-HMTS
Parathion	0.50µm	0.199	0.334
	0.75µm	0.315	0.522
Parathion-methyl	0.50µm	0.04	0.107
	0.75µm	0.077	0.148
Paraoxon	0.50µm	0.01	0.058
	0.75µm	0.023	0.098

Table A.6: Resistance sensitivities for 0.50µm and 0.75µm thick BPA-HMTS and PECH films when exposed to parathion, parathion-methyl, and paraoxon concentrations.

Sensitivity Δτ (minutes/ppm)			
Analyte	Film Thickness	PECH	BPA-HMTS
Parathion	0.50µm	49.49	31.57
	0.75µm	104.89	157.32
Parathion-methyl	0.50µm	18.24	11.72
	0.75µm	25.92	20.13
Paraoxon	0.50µm	1.04	11.89
	0.75µm	2.07	18.72

Table A.7: Normalized response time for 0.50µm and 0.75µm thick BPA-HMTS and PECH films when exposed to parathion, parathion-methyl, and paraoxon concentrations.